Engineering Structures 267 (2022) 114587

Contents lists available at ScienceDirect

Engineering Structures

journal homepage: www.elsevier.com/locate/engstruct

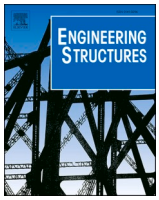

A numerical investigation of 3D structural behaviour for steel-composite structures under various travelling fire scenarios

Zhuojun Nan [a,b], Xu Dai [b,c,*], Haimin Chen [b], Stephen Welch [b], Asif Usmani [a]

[a] Department of Building Environment and Energy Engineering, The Hong Kong Polytechnic University, Hong Kong
[b] School of Engineering, The University of Edinburgh, Edinburgh, United Kingdom
[c] Fire Engineering, Buro Happold, London, United Kingdom

ARTICLE INFO

Keywords:
Performance-based engineering
Travelling fires
3D structural response simulation
Steel-composite structure
Fire resistance

ABSTRACT

In performance-based structural fire engineering, "travelling fires" is being gradually accepted as an important fire boundary condition. However, its application is still limited by uncertainties in the selection of different design travelling fire parameters, resulting from the lack of relevant experimental data and corresponding validated structural finite element models which can be used with advanced travelling fire methodologies, e.g. the Extended Travelling Fire Methodology (ETFM) framework. This paper aims to fill this gap through modelling a prototype steel-composite floor structure (representing a "slice" of a large open-plan office), to investigate its true structural response under a wide range of travelling fire scenarios, with an emphasis on considering the effect of concrete slab in a 3D finite element model, using LS-DYNA. To ensure the credibility of this numerical study, the model was first validated against the experimental data of the structural response from the Veselí Travelling Fire Test. In the parametric studies, 32 cases were examined to investigate the thermal and structural response, related to the selection of key design parameters for travelling fires (i.e. fire spread rates, fuel load densities and inverse opening factors (IOF)); fire protection (i.e. different fire protection schemes and required fire resistance rating (FRR)), and the effect of slab specification (i.e. thicknesses and steel reinforcements).

It was found that solely satisfying the critical temperature and deflection criteria for the structural members might not guarantee a sufficient structural design for travelling fire scenarios, and it is suggested that the steel stress utilisation should also be examined. Compared with the IOF, it appears that the selection of fire spread rates and fuel load densities are likely to be more critical in identifying the worst travelling fire scenario for the structural response with fire protection. Moreover, the global structural response under travelling fire is also affected by the combination of fire protection (i.e. equivalent FRR in this paper) and fire spread rate. Under a "slow" travelling fire (e.g. 0.5 mm/s) with increasing FRR, the failure of structural elements during the cooling phase was prevented effectively; however, under a relatively "fast" travelling fire (e.g. 2.5 mm/s, 12.5 mm/s), increasing FRR may not always improve the fire performance of the structure. This work also indicates that steel reinforcement ratio has a greater influence on structural response than slab thickness under travelling fires. Furthermore, the 3D finite element model is very important for structural fire analysis, not only due to the more conservative internal force captured by the 3D model (i.e. reduced by over 80 % on the 2D model in our case) thereby reproducing the collapse triggered by the failure of the connection under fire in general, but also the 3D model was able to better represent the deflection and the "internal force reversal" caused by travelling fires.

1. Introduction

For structural fire design, appropriate fire boundary conditions are critical to fire severity calculations, which may differ significantly from those in standard tests. Current practice for fire safety design of structures is often based on the prescribed provisions [1], but it is recognised that individual structural members under standard fire exposures do not provide information about the actual performance of a component or assembly in a real fire environment [2]. Performance-based structural fire engineering approaches have been published in national design codes [3,4] as desirable alternative design methods for fire resistance. With today's large open-plan compartments that are typical of modern

* Corresponding author.
E-mail addresses: x.dai@ed.ac.uk, xudai1987@gmail.com (X. Dai).

https://doi.org/10.1016/j.engstruct.2022.114587
Received 2 January 2022; Received in revised form 15 May 2022; Accepted 25 June 2022
Available online 28 July 2022

buildings, there is a significant challenge in representing the fire exposures in a manner which is accessible to practitioners. This kind of problem has been tackled using "travelling fire" methodologies in recent years, a concept which invokes fires that may burn locally and spread by "travelling" across entire floor plates over a period of time, in larger compartments [5,6]. Further discussion is necessary regarding the application of the "travelling fire" methodology in performance-based structural fire engineering, namely, the effects of "travelling fire" on thermal and structural response.

1.1. Travelling fires

The "travelling" nature of fire and non-uniform temperature distribution within the large open-plan compartments has been observed in many fire accidents, such as those in the World Trade Center Towers 1, 2 & 7 (2001) [7], the Windsor Tower (2005) [8], the Faculty of Architecture Building at the Delft University of Technology (2008) [9], and the Plasco Building (2018) [10,11]. Moreover, some of these buildings partially or fully collapsed, such as the WTC Tower 7 where the large compartment was observed to support a "travelling" burning zone [7]. As part of an investigation into the mechanisms leading to collapse of World Trade Center Towers 1 & 2, the National Institute of Standards and Technology (NIST) reconstructed the potential fire impact inside building compartments [7]. The high levels of temperature inhomogeneity in the large compartments was reported where such developing/spreading fires occurred [7]. It was concluded that resorting to compartment temperature averaging may lead to significant errors in the thermal and structural response, since the fire conditions were probably highly variable spatially [5,6]. This underlines the potential role of "travelling" fires in modern constructions that may pose severe challenges to current structural fire safe design practice.

"Travelling" fires in large open-plan compartments may result in the complexity and interconnectedness of the structural fire behaviour that can be highly unpredictable. Since the 1990 s, over ten full-scale travelling fire experiments have been conducted to reproduce the non-homogeneous temperature distribution and investigate travelling fire behaviours in large compartments. The literature reviews for the full-scale travelling fire experiments before 2015 [12,26,60,71–73] were carried out by Stern-Gottfried & Rein [5] and Dai et al. [6]. In very recent years, there are additional full-scale travelling fire tests, e.g. the Malveira Fire Test (2014) [13], the large-scale travelling fire experiment series from European RFCS TRAFIR project (2017–2020) [14,15], and the x-ONE and x-TWO (2017, 2019) [16]. These recent tests identified different modes of fire spread in the large open space, and provided valuable data for the travelling fire key design parameters, i.e. ventilation conditions and fuel load distributions. Those experimental results further confirmed the deficiency of current structural fire design without considering the travelling fires.

A series of theoretical representations of travelling fire models have been developed in response to related fire accident investigation and experimental results, hereinafter referred to as Clifton's travelling fire model [17], Travelling Fires Methodology (TFM) [5,18] and its subsequent refined versions (i.e. Improved Travelling Fires Methodology (iTFM) [19] and Travelling Fires Methodology with flame extension (fTFM) [20]), and the Extended Travelling Fire Methodology (ETFM) framework [6,21,22]. Different from other travelling fire methods, the ETFM framework is postulated on a "mobilised" version of Hasemi's localised fire model [24] for the fire plume near the structure (i.e. near-field), combined with a simple smoke layer calculation using the FIRM zone model for the areas of the compartment away from the fire (i.e. far-field) [25]. More importantly, the ETFM framework considers both energy and mass conservation for the fire design of the large compartment. Furthermore, Dai et al. [22] confirmed the capability of the ETFM framework in reproducing the thermal responses of the structural elements under travelling fire scenarios against the Veselí Travelling Fire Test [26], although only limited parametric studies were carried out to quantify the impact of travelling fire design parameters. This work showed that the IOF and the total heat loss are likely to be the most critical parameters for structural fire design under travelling fires [22].

To achieve the application of travelling fire scenarios in practice, further investigation of the input parameters for the ETFM framework should be carried out, e.g. travelling fire spread rates, fuel load densities, and opening factors, etc., as a focus of the current study. Performing Computational Fluid Dynamics (CFD) might be another alternative method [26–28] to characterise the fire severity for structural design. However, due to the massive computational demands, CFD might not be feasible on a day-to-day routine design basis for structural engineers. Moreover, the very detailed outputs that CFD models generate are necessarily tied to very specific definitions of the fire source and will typically embed excessive amounts of detail, which may be unwarranted for the purposes of defining sufficient thermal boundary conditions. And despite this level of detail, uncertainties in the sufficiency of the model representations, e.g. combustion over complex fuel beds, will remain high, requiring expert knowledge for interpretation, thus there is a strong indication that simplified approaches will be more useful for design purposes. Professional fire science knowledge is also required to interpret and judge results derived from complex fire scenarios. Hence, the ETFM framework is recommended as a simple design framework, which was developed to be implemented easily for structural fire performance-based design in a practical manner, thereby enabling the structural engineers to utilise a general fire-structure coupling concept without resorting to excessively large and complex simulations. Meanwhile, the ETFM framework in principle addresses more of the fire dynamics and provides a more fire science-bounded travelling fire model that incorporates mass and energy conservation.

1.2. Structural analysis under travelling fires

By the same token, a poor structural model cannot compensate for a rigorous fire model, as is the prevailing situation for travelling fires for performance-based structural engineering. For instance, Bailey et al. in 1996 [29], and Moss & Clifton in 2004 [30] systematically investigated the behaviour of steel-framed buildings under "spreading fires" (i.e. so-called "travelling fires" nowadays). However, the travelling fire model applied in those studies was rather crude, essentially a series of parametric fires with a time lag. More recently, the TFM [5,18] has been applied to investigate the effects of travelling fires on the structural response of the different structural systems, i.e. steel frame [18,23,38,39], concrete structure [33,34], and composite construction [32,35]. These studies concluded that the single worst-case fire scenario cannot be readily identified, i.e. it is important to consider various fire scenarios, both uniform and non-uniform to achieve the comprehensive analysis of the structural responses and failure modes. These findings also revealed that the travelling nature of fire, the extended travelling fire duration and the structural types are the vital factors affecting the differences between uniform fires and travelling fires. The TFM was implemented in the OpenSEES software framework [36] by Jiang et al., and the effects of travelling fires on the thermal responses of a large composite structure were studied [37]. The results showed that travelling fires with larger size (25–42 % of the floor area) might lead to earlier failure of steel beams, while travelling fires with smaller size could produce higher peak temperatures in the concrete slab.

It is worth noting that the majority of the previous numerical studies on travelling fires [29–35,37] lacked structural model validation under a travelling fire scenario. This was mainly due to the limited availability of experimental data, i.e. that which well characterised both the travelling fire behaviour and the resultant structural response [6]. Rezvani & Ronagh in 2015 [38] and Rackauskaite et al. in 2017 and 2019 [23,39,40] performed extensive numerical studies on structural response of steel-framed buildings, using 2D generic frame structures under the TFM [5,18] and its subsequent refined version iTFM [19]. These studies are practically of limited value, as a travelling or spreading

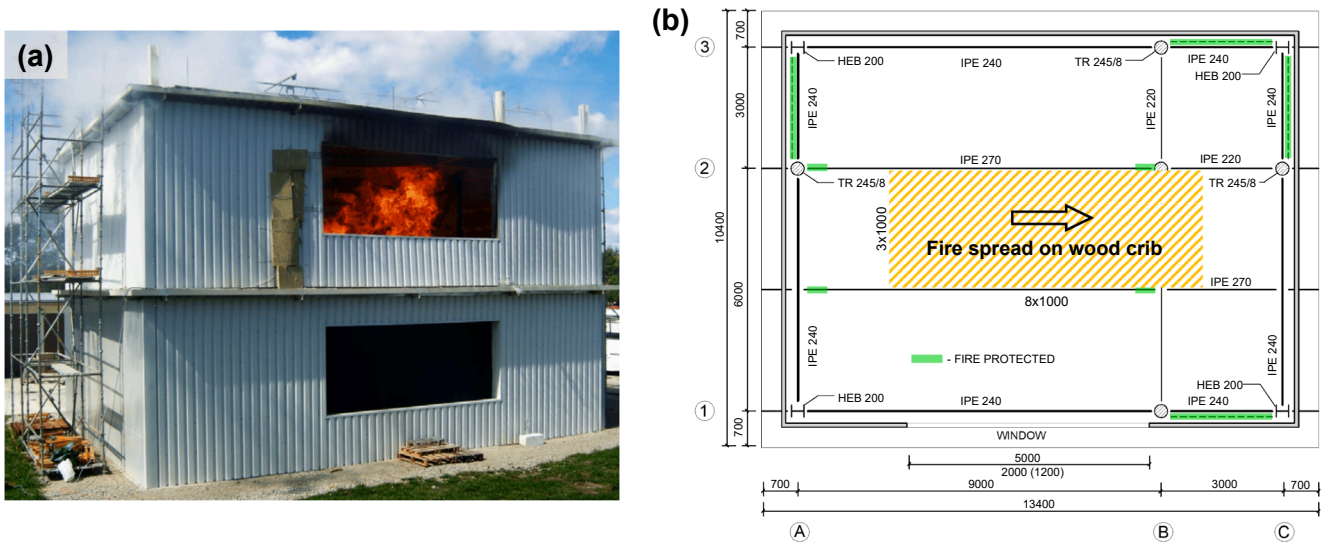

Fig. 1. (a). Photo of the fire progression during the Veselí Travelling Fire Test on the upper floor; and (b). Plan view of upper floor structural layout and wood crib distribution (unit in mm). (both figures adapted from Horová et al. [26]).

fire is by its nature a 3D phenomenon and 2D structural models simply cannot represent the complexity of behaviours presented in a realistic structure, such as the membrane behaviour of floor systems. The Cardington fire tests clearly showed that the slabs carried most of the load at very high temperatures [41].

The performances of 2D and 3D model structures exposed to traditional fire boundary conditions (i.e. either uniform heating or localised fire), have been examined in various studies [42–45]. Junior et al. [42] compared 2D and 3D numerical modelling analysis of a single storey industrial building under uniform heating. The 2D model was found to be unrealistic, since it failed to capture the lateral instability of the portal member. Quiel and Garlock [43] compared the predicted behaviour of high-rise steel frames under fire using 2D and 3D models. The results showed that the two models capture similar thermal responses but that the continuous slab had a non-negligible effect on the member's deflection. Jiang and Li [44,45] compared the progressive collapse analysis of steel frames with concrete slabs exposed to localised fire between 2D and 3D models. The results demonstrated that the collapse modes and load redistribution path of the 2D model and 3D model were different: the loads previously sustained by the buckled heated column were transferred more along the short span rather than the long span. The presence of slabs in the 3D model delayed the global collapse. Therefore, the 2D model produces more conservative results by underestimating the collapse resistance of structures.

More recently, several studies have been conducted on 3D structural models to investigate the mechanical responses under travelling fires. Martinez and Jeffers [46] performed a computational investigation using a 3D structural model with slabs. Although only one travelling fire scenario was adopted, the simulation results revealed the dependency of the slab vertical displacement rate and the maximum vertical displacement upon both the fire origin and the extent of the travelling fire burning region. Rezvani et al. [47] assessed the robustness of a generic four-storey moment-resisting steel structure with one-hour FRR exposed to travelling fire with various fire sizes. The investigations demonstrated that the fire protection system based on the requirements of standard fire tests may not be adequate with real fires (e.g. travelling fires).

An iterative design procedure for performance-based design of composite steel buildings was recommended by Gernay and Khorasani [48], in that systematic design changes were introduced to address the observed failure modes. Fire-structure behaviour for multiple design alternatives and hazard scenarios can be examined using performance-based fire design. This research revealed that only the full building model can realistically be used for multi-compartment fire (i.e. travelling fire) and multi-hazard fire after column loss. More specifically, the simulation results showed that the increase of the steel reinforcement mesh in the concrete slab is needed to achieve resistance to full burn-out under extreme events.

Jiang et al. [49] investigated the disproportionate collapse of 3D steel-framed gravity buildings under travelling fires. It was found that a higher level of fire protection may prevent the collapse of structures, but may also lead to collapse in the cooling phase due to the delayed increment of temperatures in the heated members. However, only three travelling fire scenarios (i.e. different fire curves and spreading rates) were examined, using Clifton's travelling fire model. A more sophisticated travelling fire model, ideally based upon energy and mass conservation of the large compartment, is needed to investigate the structural global behaviour under various travelling fire scenarios systematically. Besides, no secondary beams were modelled in the structural and heat transfer models in this study [49]. However, fire protection is actually required for all structural steel members in the conventional fire resistance design. The investigation of the effect of fire protection removal from the secondary beams on the thermal-mechanical responses of the steel frame with composite floors under travelling fires is still needed.

1.3. Research objectives

This paper aims to identify the importance of concrete slab inclusion with a 3D structural model for steel-composite structures under travelling fires, with a special emphasis on its different structural implications compared with a 2D structural model. Further, a validated structural model is developed and applied under a more advanced travelling fire model (i.e. the ETFM framework) via various travelling fire scenarios. Such extensive analysis is to identify which travelling fire design parameters (i.e. fire spread rate, fuel load density, and opening factor), or related structural design parameters (i.e. fire protection, slab thickness and steel reinforcement), are more critical to achieve a safe structural fire design. The importance of different failure criteria (i.e. critical temperature, deflection or deflection rate, and stress utilisation) are also assessed to identify their importance in reference to the practical performance-based design.

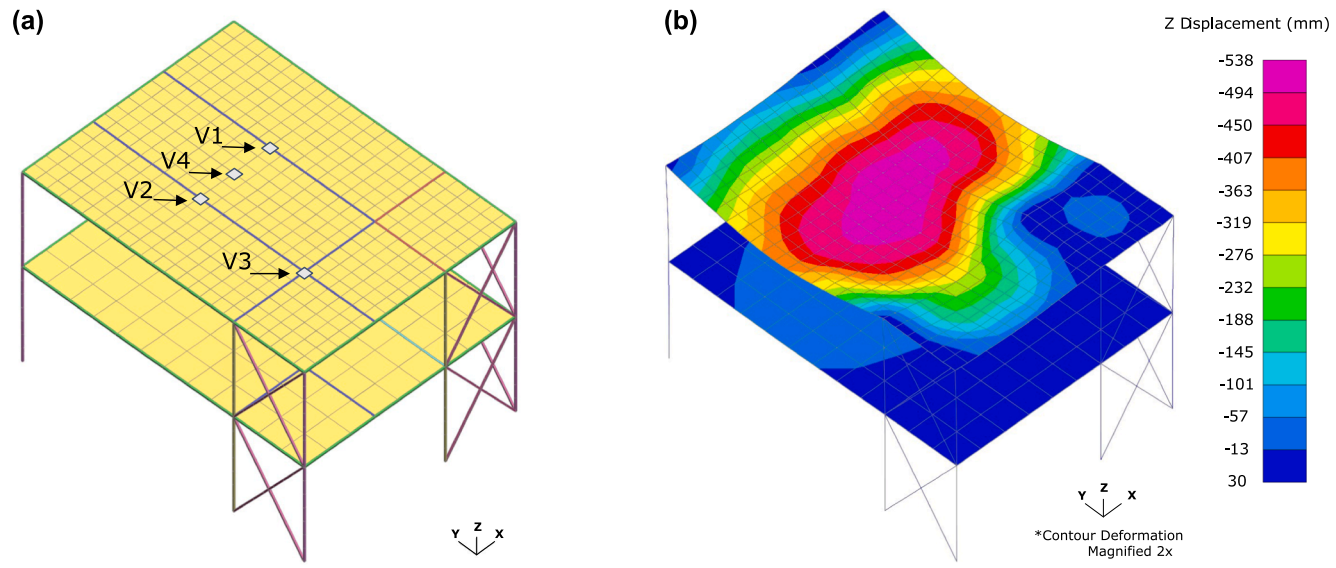

Fig. 2. (a). 3D finite element model of the Veselí Travelling Fire Test building (tags V1 to V4 are monitored locations for comparison in Fig. 3); and (b). Displacement contour of the model while reaching its maximum deflection (2 times scaled).

2. Validation of the structural model - Veselí Travelling Fire Test

According to the literature, there are very few full-scale structural fire experiments aimed at the characterisation of both the structural response and the travelling fire behaviour; one notable exception is the Veselí Travelling Fire Test carried out in 2011 in the Czech Republic [26]. The experimental compartment is a two-story steel framed building with composite floors, which had two by three bays in plan (13.4 m × 10.4 m) with a total building height of 9.0 m, see Fig. 1(a).

2.1. Structural model

In the Veselí Travelling Fire Test, the columns of the upper floor used HEB 200 and TR 245/8 filled with concrete C30/37, and the steel beams had dimensions of IPE 220, IPE 240, and IPE 270 (steel S355) respectively, see Fig. 1(b). The ceiling floor was composite with trapezoidal steel sheets (thickness 0.75 mm, S350), and the total thickness of the ceiling slab was 100 mm in the upper floor. The composite ceiling floor had steel wires ø 1 mm length of 60 mm with average tensile strength of 1450 N/mm^2, in quantities 30 kg/m^3 [50]. It is important to note that the ceiling floor was not subject to any other mechanical loading except for its self-weight, which is equivalent to approximately 1.68 kN/m^2. Fin plates and reverse channel connections were designed to resist shear forces. Two cross bracings were used for providing building horizontal stiffness.

In this paper, an explicit dynamic analysis was performed for structural responses under travelling fires. In the LS-DYNA finite element structural model [52], the formulation of steel structural elements was Hughes-Liu type with cross section integration and the number of integration points in the cross-section was 21. The Young's modulus and yield strength of steel elements were taken to be 210 GPa and 355 MPa, respectively. The material of steel beams used MAT_202: Steel_EC3, and thermal properties for MAT_202 were defined according to EC3 [53]. Considering the concrete-filled steel columns were protected in the experiment, besides the main research interest of this validation study is regarding the deflections of the steel composite floor system at mid-span under a travelling fire, hence the concrete-filled steel internal columns (TR 245/8) were simplified to steel tubular columns in the LS-DYNA model. Note that similar simplification was also applied by Horová and Wald [54] for the Vulcan model, i.e., the concrete-filled steel internal columns were simplified to steel columns with I-section. The impact of such simplification on the thermal response is negligible for a protected column. The Cofraplus 60 composite slab in the upper floor was simplified as the equivalent self-weight of flat concrete slab with a continuous depth of 70 mm, reinforced by two layers of reinforcement mesh ø 5 mm 196 mm^2/1000 mm placed 30 mm from the top of the cross-section [54]. The strength of reinforcements was 420 N/mm^2. The shell element formulation of slabs was Belytschko-Lin-Tsay, which is computationally efficient for the explicit dynamic solver of LS-DYNA. The slab was modelled by a layered composite shell formulation, in which a distinct structural material, thermal material, and thickness can be specified for each layer (*PART_COMPOSITE). The material type of C30/37 concrete slabs was MAT_172: CONCRETE_EC2. The thermal properties of concrete were defined according to EC2 [55].

The unfactored design loads were applied as the mechanical loading according to the experiment setup [50]. A total self-weight of 1.68 kN/m^2 from the concrete slab was applied on the upper floor. The self-weight of the lower floor was 2.04 kN/m^2 from the 120 mm thickness concrete slab. Two different types of connections, rigid and pinned, were considered to demonstrate the effects of connections on determining the validity of this LS-DYNA finite element model. To avoid the symmetric problem, an initial imperfection (horizontal point loads equal to 1/1000 of the axial force in the columns) is applied at the top of the columns [45,51]. The shell element size was 0.5 m × 0.5 m, and 1.0 m × 1.0 m for the upper floor slab and lower floor slab respectively. The mesh size of the beam was the same as the shell elements on different floors. The columns were discretized with 7 elements, and the column element size was around 0.57 m (Fig. 2(a)). A mesh-sensitivity analysis was performed to investigate the extent to which the element size could be increased while maintaining sufficient accuracy. Three alternative meshes were considered for the upper floor slab, which are 0.25 m × 0.25 m, 0.5 m × 0.5 m, and 1.0 m × 1.0 m. The largest discrepancy between the 0.5 m × 0.5 m mesh and the 1.0 m × 1.0 m mesh results was 64 %, in terms of location V4. For the 0.25 m × 0.25 m mesh and the 0.5 m × 0.5 m mesh, the mesh size has little effect (<10 %) on the results. The element size of 0.5 m × 0.5 m was used for the upper floor slab to maximise the computational efficiency. Another sensitivity analysis was also carried out to determine the appropriate timescale. It was shown that the duration of travelling fire can be scaled by a time factor of 1/1000 for the explicit dynamic analysis in LS-DYNA.

2.2. Fire boundary

In the Veselí Travelling Fire Test, wood crib fuel bed was uniformly

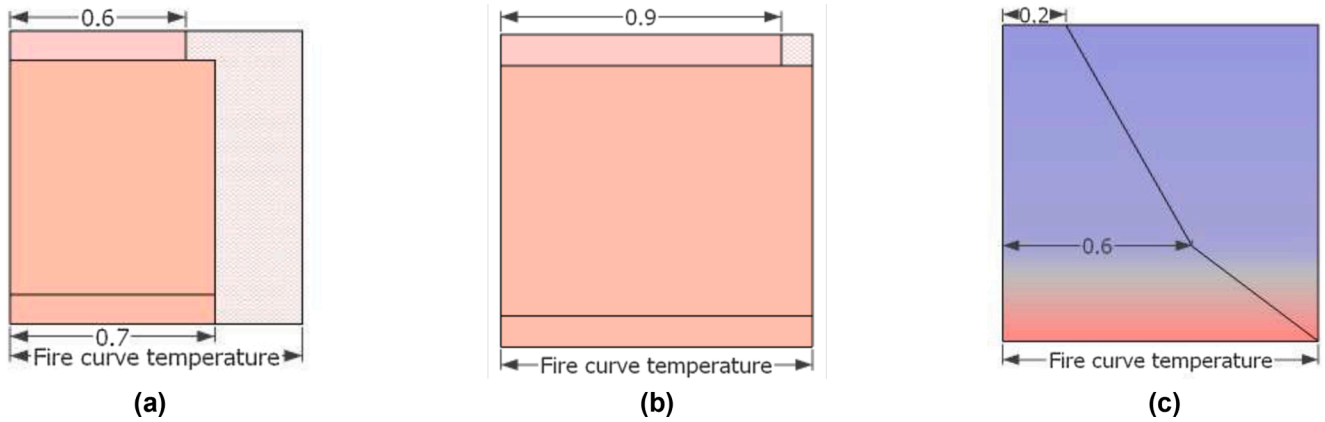

Fig. 3. The temperature patterns for cross-sectional heat transfer analysis [54]: (a). Protected beam; (b). Unprotected beam; and (c). Floor slab.

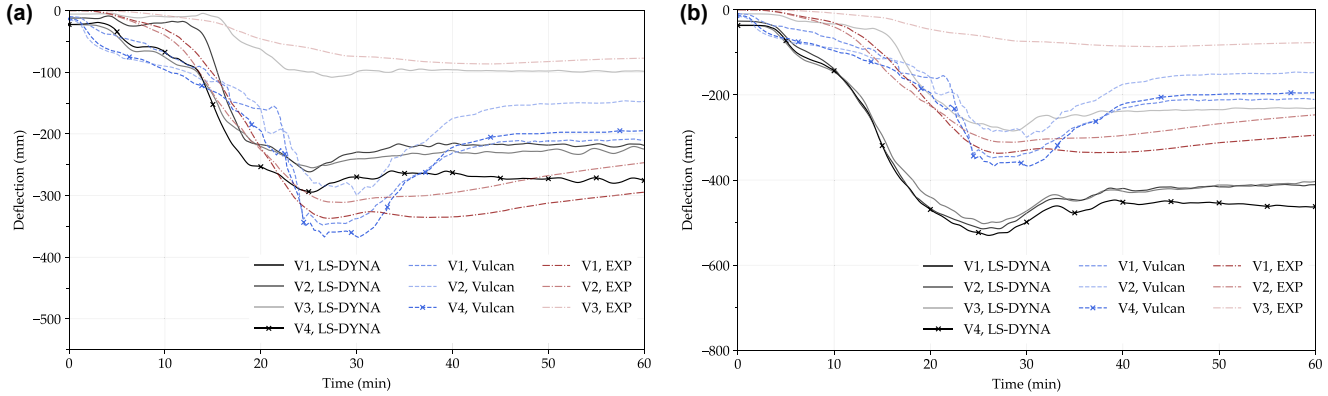

Fig. 4. Deflection comparison between the Veselí Travelling Fire Test data, the Vulcan modelling data [54], and the LS-DYNA finite element modelling results, at various locations V1 to V4, when assuming: (a). Connection rigidity - fixed; and (b). Connection rigidity - pinned.

distributed in a rectangular shape, with dimensions of 3 m × 8 m, at the centre of the test compartment. Its equivalent fire load density on the whole floor area was 173.5 MJ/m^2. The wood crib was ignited with a linear source at the left end, hence the fire could develop naturally in a "travelling" fire manner. More details of the Veselí Travelling Fire Test can be found in reference [50].

To minimise the comparison uncertainty between the structural model prediction and the experimentally measured structural response, the measured thermocouple time-temperatures of TG2-TG4, TG6-TG13, and TG14-TG20, from the gas phase, were applied to the related parts of the structural elements close to the locations of these sensors. Those time-temperature histories were multiplied with certain reduction ratios to consider the heat transfer within the structural member cross-sections following the assumptions by Horová and Wald in 2015 [54]. Fig. 3 presents such temperature reduction patterns with certain ratios, which were originally benchmarked for numerical model simplification on structural fire engineering in general by Wald et al. [76]. For example, the temperature reduction ratios 0.7 and 0.6, were applied on the fire exposed surface and the unexposed surface of protected steel beams.

2.3. Model validation

Fig. 4 presents the validation of the LS-DYNA structural finite element model against the experimentally measured steel beam deflections, and the Vulcan modelling results from Horová and Wald [54]. For expediency, the fin plates and reverse channel connections were simplified as either fixed (Fig. 4(a)), or pinned (Fig. 4(b)) to represent the connection rigidity. It can be seen that both models capture the structural deflection sequence when the fire travels, i.e. V1, V2, and V4 start to deflect as a group first, as they are closer to the travelling fire ignition source, and displacement of V3 at the far end of the compartment starts to increase with approx. 5 mins time delay. This deflection sequence was also captured by the experiment. It is worth noting that V1 of the LS-DYNA model reached its maximum 261 mm at 25 mins with the rigid connection, and 515 mm at 25.5 mins with the pinned connection, and results (V1) from the experiment showed that its maximum value at 27 mins with 340 mm, which lies in-between the two LS-DYNA model predictions. This is consistent with the expectation that in reality the connections should have a certain level of rotational stiffness, although the fin plates and the reverse channel connections were designed to resist the shear force only [56]. The structural residual deflection during the cooling phase was also properly reproduced by the two LS-DYNA models.

3. A prototype steel framed composite structure under the baseline travelling fire scenario

Although the finite element structural model was validated against the Veselí Travelling Fire Test [26,50] and other similar modelling efforts [54], it is important to note that the aspect ratio of the test compartment was close to 1, i.e. approx. 1.3 obtained by 13.4 m over 10.4 m. This low aspect ratio is not ideal for carrying out parametric studies for travelling fire scenarios, as both the thermal and structural response of the structural members along the fire travelling trajectory are not very distinguishable in terms of time lag [22,26,54]. Hence, it is of value to further adapt the validated LS-DYNA 3D finite element structural model for the Veselí Travelling Fire Test to a prototype steel framed building which has a much higher compartment aspect ratio, i.e.

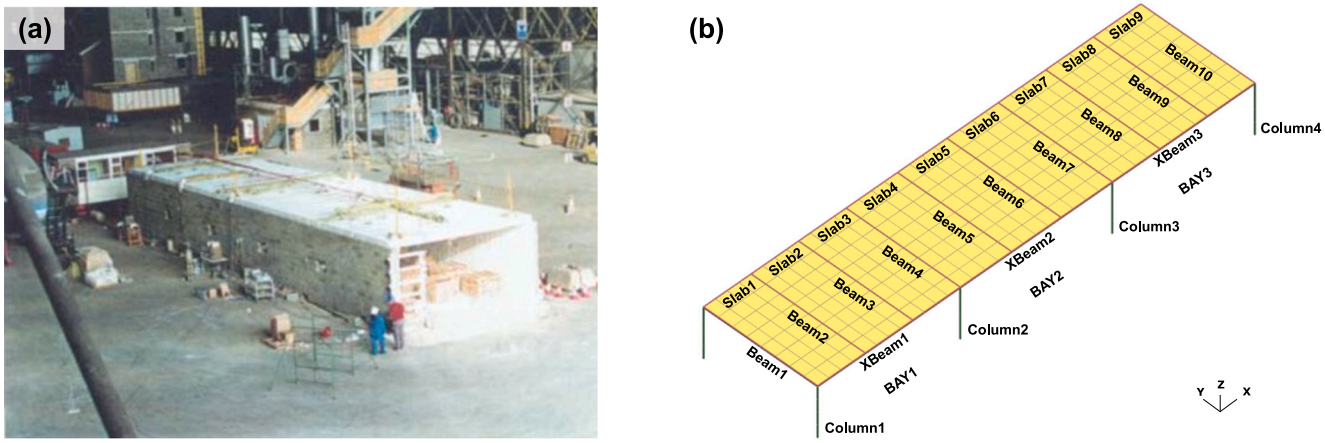

Fig. 5. (a). Test compartment of the BST/FRS 1993 Fire Test Series [12]; and (b). 3D finite element model of the newly adapted prototype building (beams and slabs tagged for reference).

a long slim shape. Inspired by the structural layout of the BST/FRS 1993 travelling fire test (performed within a "slice" of the large open-plan office compartment, see Fig. 5(a)) [12], the adapted new LS-DYNA 3D numerical model represents a one-storey prototype steel-framed building with composite floors, having structural dimensions of 23 m length × 6 m width × 2.75 m height, see Fig. 5(b). This prototype steel framed building has three bays: the first bay and third bay have the same length of 7.5 m, which are slightly shorter than the length of the second bay, i.e. 8 m.

3.1. Modelling of the prototype structure

This prototype structure was designed following the Eurocode [57] to resist an ambient design load on the floor (1.35 × dead load + 1.5 × live load = 1.35 × 4.13 + 1.5 × 2.5 = 9.3 kN/m^2). Note that the unfactored design loads were used as the combination for the fire limit state [23]. The cross-section of all floor beams and columns was chosen as UB 406 × 178 × 54 with steel grade S355. The designed composite slabs were composed of trapezoidal sheets Cofraplus 60 [58] (thickness 1.0 mm, steel S350) and concrete C30/37. The total thickness of the

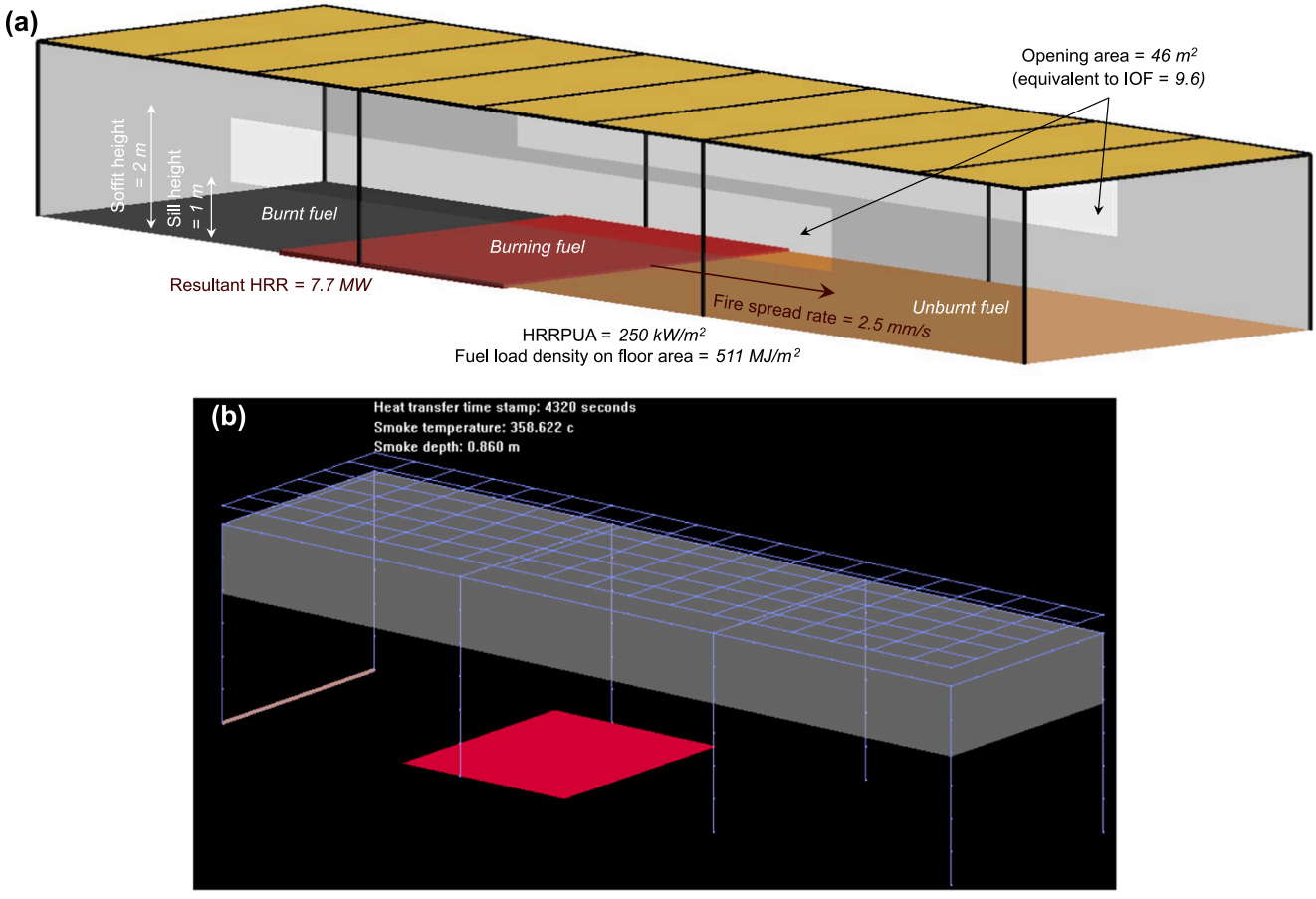

Fig. 6. The demonstration of travelling fire via the baseline fire scenario: (a). The schematic with the input parameters; and (b). The automatic rendering while carrying out the fire modelling in OpenSEES/SIFBuilder.

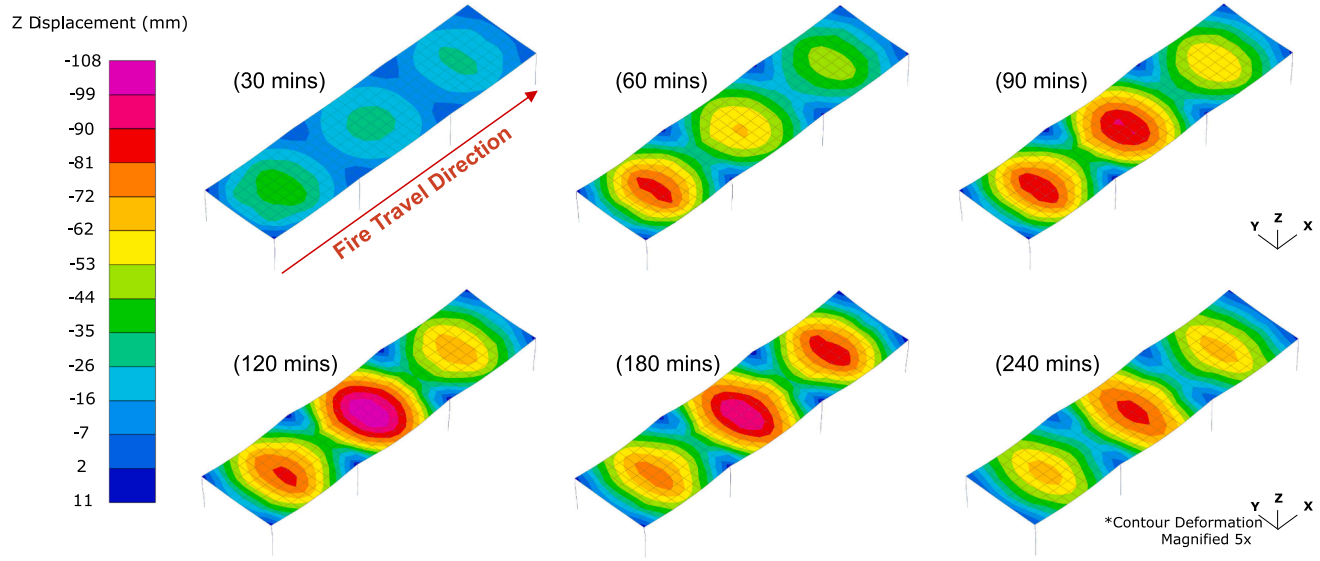

Fig. 7. The displacement development under the baseline travelling fire scenario with 5 times scaled (fire spread rate: 2.5 mm/s, fuel load density: 511 MJ/m^2, HRRPUA: 250 kW/m^2, and IOF: 9.6).

composite floor was 140 mm. The overall steel rebar mesh B503 (ø 8 mm 100/200 mm) was placed 25 mm from the top and ø 8 mm reinforcement was used in each rib with the strength of 420 N/mm^2. For the composite floor, the same simplification method used in the Veselí validation model was adopted. The Cofraplus 60 composite slab was simplified as the equivalent self-weight of flat concrete slab with a continuous depth of 110 mm, reinforced by structural mesh fabric B503 (i.e. 503 mm^2/1000 mm) including two layers of ribbed mesh ø 8 mm with the strength of 420 N/mm^2. The two layers of reinforcement were placed 25 mm from the top and the bottom of the slab cross-section, respectively. All steel beams (including secondary beams and primary beams) and columns were designed for one-hour FRR, using mineral fibre spray of 15 mm thickness with thermal conductivity 0.12 W/(mK), density 300 kg/m^3 and specific heat 1200 J/(kgK) following the recommendations from Franssen et al. in 2009 [1]. During the fire simulation, the load imposed on the beams was in the range of 0.2 to 0.4 of their ambient design capacities. Both the travelling fire modelling and subsequent heat transfer analysis were carried out using OpenSEES [22]. Note that all the connections were modelled as pinned instead of rigid, as the former generally provides a more conservative structural response. Mesh sensitivity study was performed, suggesting the size of 0.625 m × 0.75 m for shell element, the size of 0.6875 m for column element, and the length of beam element was in accordance with the shell element.

3.2. The baseline travelling fire scenario using the ETFM framework

To carry out the parametric studies of the structural response under various travelling fire scenarios, a baseline case has to be defined first. The selection of this baseline travelling fire scenario (see Fig. 6) follows the rules that the relevant design parameters are from common design practice. Meanwhile, it is required that this selected baseline fire scenario can challenge the prototype steel framed building close to its "failure", i.e. either following the critical temperature criteria, or the maximum deflection (rate) criteria. Hence, a well distributed "spectrum" of the structural response can be explored in the subsequent parametric studies.

Fuel load density of 511 MJ/m^2, and heat release rate per unit area (HRRPUA) 250 kW/m^2, were selected for office buildings following Eurocode 1 [59]. Fire spread rate was assumed to be a constant 2.5 mm/s, which was within the typical range between 0.1 and 19.3 mm/s based on the previous experimental results [19] and also could determine a fairly large fire size (i.e. 7.7 MW) in the ETFM framework. In addition, the total heat loss fraction 0.85 was adopted including a constant

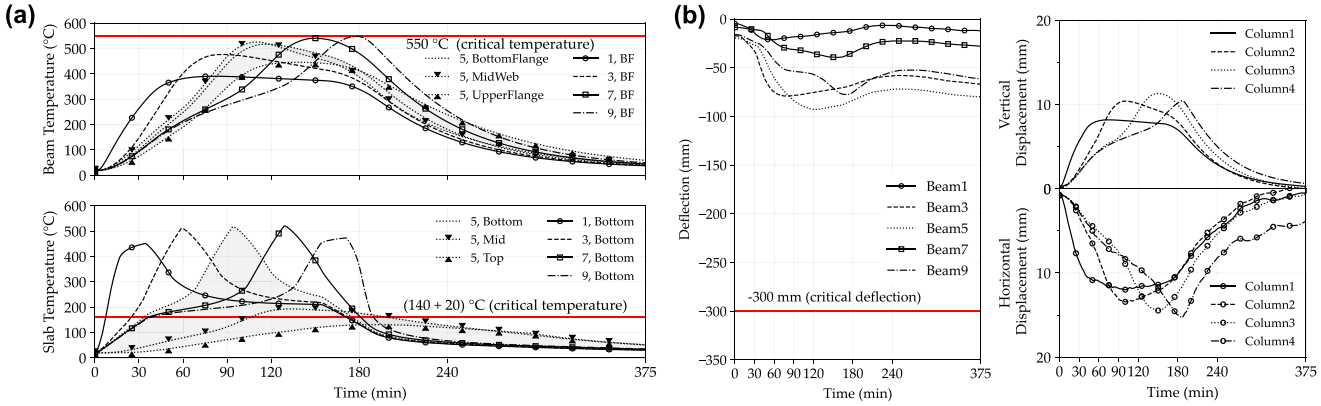

Fig. 8. Thermal and mechanical response of the structural elements under the baseline travelling fire scenario, Beam1 - Beam10 and Slab1 - Slab9: (a). Temperature development; and (b). Deflection of the beams at mid-span and displacement of the columns head.

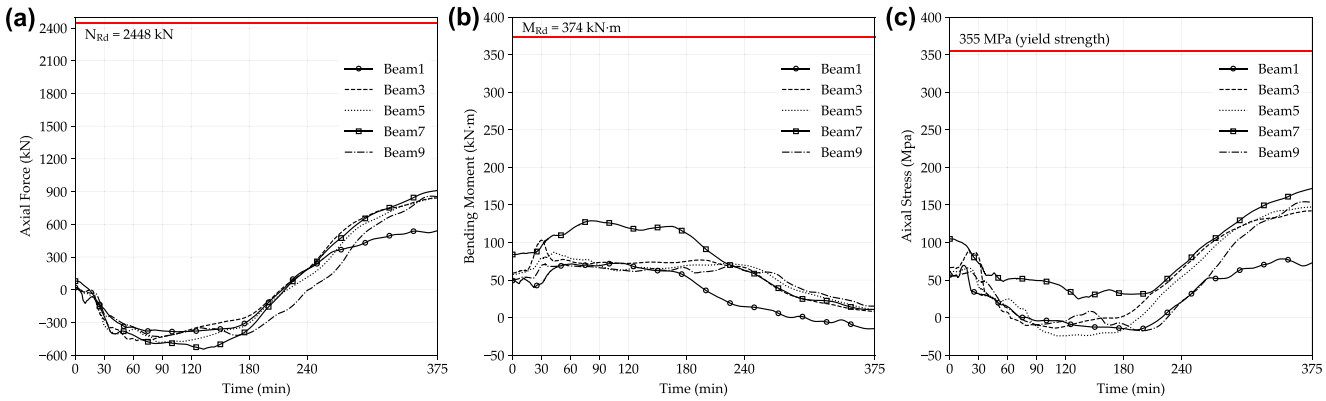

Fig. 9. Internal force and stress of the beams at mid-span under the baseline travelling fire scenario, Beam1 - Beam10: (a). Axial force; (b). Bending moment; and (c). Axial stress of lower flange.

radiative heat loss fraction of 0.35 following the suggestions by Janssens [25]. Two openings with dimensions of 14 m × 1 m were assumed on the "long" sides of this large compartment, having sill height 1 m and soffit height 2 m (see Fig. 6). This opening assumption is equivalent to an IOF of 9.6, which is a suggested intermediate value in the region between fuel-controlled and ventilation-controlled burning, following Thomas & Heselden [61] and Dai et al. [22]. The fire was assumed to start at one short end of the compartment, travelling along the longitudinal direction.

3.3. Thermal and structural responses under the baseline scenario

Note that a Python script [74] was developed for interfacing the OpenSEES/SIFBuilder [21] generated thermal analysis (i.e., fire modelling from ETFM framework and heat transfer analysis), with the subsequent thermo-mechanical analysis using LS-DYNA. This script efficiently bridges the information between two software and supports extensive parametric studies presented in later sections.

Fig. 7 presents the slab deflection contour development under the baseline travelling fire scenario every 30 mins. Generally, the deflection sequence of the steel beams in those three bays followed the travelling fire trajectory, i.e. as the fire travelled through each bay it would have the largest deflection compared to the other two bays; and as the fire travelled away from it, deflection would decrease due to cooling. Interestingly, the second bay, which has a slightly longer length, 8 m, had the largest residual deflection compared to the other two bays which are 7.5 m in length. This is because the longer primary beams of the second bay generated larger deflections in the heating phase due to their thermal expansion being restrained by the neighbouring cooler bays, and hence relatively larger residual deflection occurred during the cooling phase.

Fig. 8(a) summarises the time-temperature histories of the beams and slabs along the travelling fire path. In Fig. 8(a), it can be seen that Beam9, located at the far end of this longitudinal compartment, experienced the maximum member temperature 550 °C at 178 min. It reached critical temperature 550 °C, which was assumed for composite beams supporting concrete floor slabs when the building occupancy is not specified [77]. This is due to the effect of the far-field smoke temperature, which preheated the steel member for a long time, allowing the heat to penetrate through the fire protection, eventually reaching its maximum value, when the near-field fire reached the third bay. In contrast, Beam1 had a lower peak steel member temperature, i.e. 390 °C, as this beam was close to the travelling fire ignition location. When the near-field travelling fire left the first bay, only far-field smoke was left to heat this structural element. Fig. 8(a) shows the temperatures in the concrete slabs, and it should be noted that none of the slab top surfaces reached its critical temperature, i.e., 160 °C, which is defined based on the ASTM E119 [78].

The structural deflection history of the beams followed the same trend, i.e. Beam1 had the lowest deflection, 21 mm at 57 min, in contrast Beam5 had the largest deflection 93 mm at 124 min due to the larger deflection of the primary beams in the second bay. In addition, none of the beam members reached their critical deflection of 300 mm, i.e. L/20, where L was the beam member length of 6 m, as shown in Fig. 8(b). Fig. 8(b) presents the vertical and horizontal displacements of the column head. The head of Column4 had the largest horizontal displacement of 15 mm at 186 min. This column was connected to Beam10 located at the very far end of the prototype structure. The higher temperature (around 550 °C) induced larger axial thermal expansion of Beam10, which was shown as the largest horizontal displacement of Column4 head, resulting in larger axial forces in the connections, which also potentially challenged the connections at the far end of the prototype structure. This finding implies the fire ignition location might also potentially influence the structural response and subsequent structural failure modes, which requires further systematic study. Note that the vertical thermal expansion of the columns caused the decreasing absolute displacement of the beams. The horizontal displacement of the columns measured at the top end of the columns also indicates the axial thermal expansions and contractions of the corresponding primary beams. The range of horizontal thermal expansions was between 10 mm and 15 mm.

Fig. 9 summarises the internal forces and stress histories of the steel beams along the travelling fire path. Positive axial force represents beams in tension, and positive bending moment represents tension in the bottom surface fibre of the structural members. In Fig. 9(a), all beams experienced "axial force reversal" sequentially [62], i.e. the beams were in compression during the heating phase and in tension during the cooling phase, due to the moving of the travelling fire near-field below those steel beams. Beam7 had the largest axial force, 545 kN (in compression) and 910 kN (in tension) at 133 min and 375 min respectively, and the largest bending moment at the mid-span 129 kNm at 85 min. Beam7 is likely to be under the most unfavourable internal force because: 1) Beam7 is a primary beam which tends to bear more load compared with the secondary beams; 2) Beam7 carries the loading from both BAY2 and BAY3, in which BAY2 has a slightly longer dimension compared to BAY3 (i.e. 8 m and 7.5 m respectively); 3) considering the coupling effect of the thermal and structural responses, Beam7 experienced smoke pre-heating for a sufficiently long period, so when the near-field fire travelled through, the peak temperature of Beam7 reached 550 °C. It is worth noting that the axial forces and the bending moments of all beams were both lower than the plastic compression/tension resistance $N_{Rd} = 2448$ kN and the plastic bending resistance $M_{Rd} = 374$ kNm. More importantly, as presented in Fig. 9(c), most of the steel beams (except for Beam1) had their axial stresses of lower flange exceeding 145 MPa, as the large tensile force was inevitably induced during the travelling fire cooling phase. Note that Beam1 had relatively lower

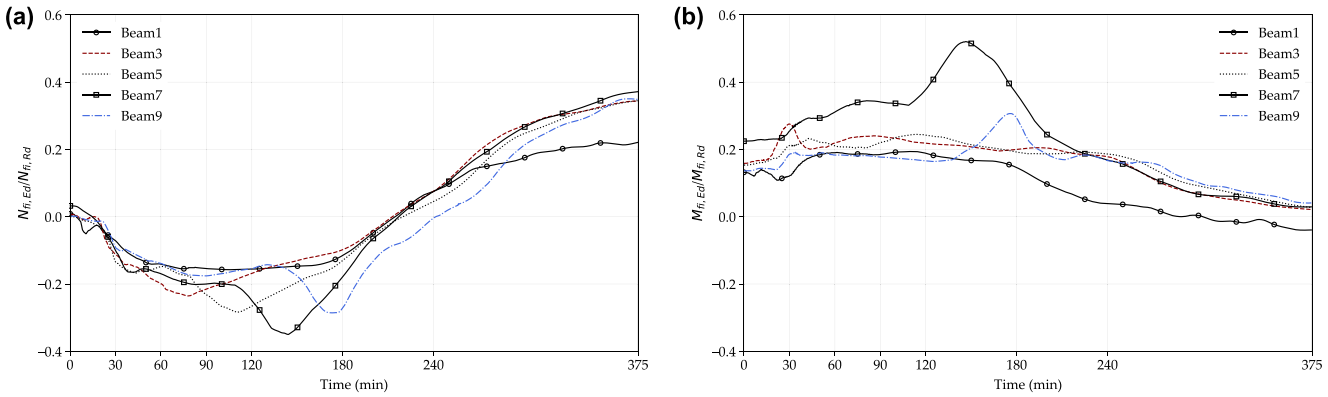

Fig. 10. Beam load-bearing capacity at mid-span under the baseline travelling fire scenario: (a). Utilisation for the tension/compression resistance; and (b). Utilisation for the bending resistance.

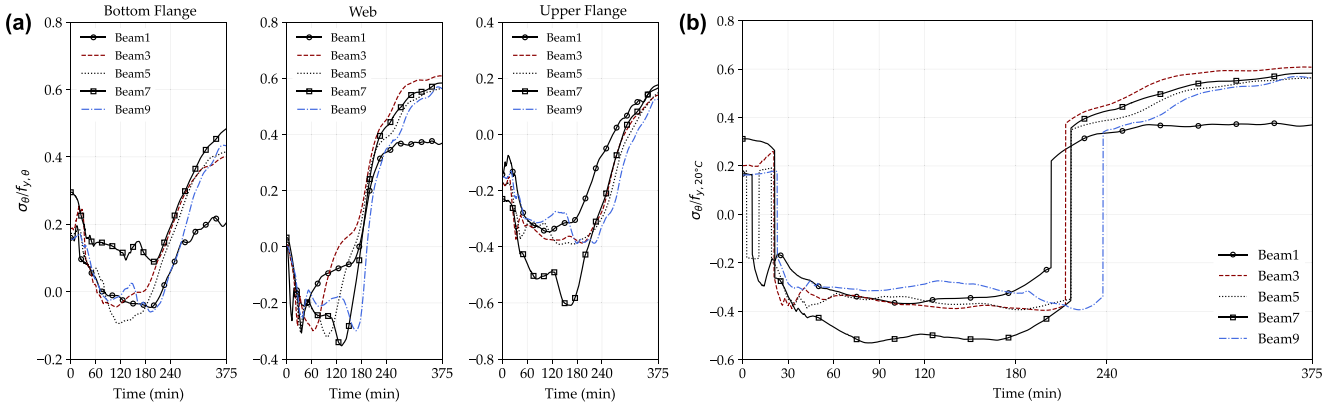

Fig. 11. Beam stress utilisation at mid-span under the baseline travelling fire scenario: (a). Ratio of axial stress at beam bottom flange, mid-web and upper flange, over the temperature-dependent yield stress; and (b). Ratio of the axial stress envelope in the beam section over the yield strength 355 MPa at 20 °C.

tensile forces compared with other beams, because it was close to the fire ignition location and acted as an edge beam of the whole prototype structure, implying this beam had both lower thermal loading (max. 390 °C) and mechanical loading (only from BAY1).

Fig. 10 presents the load-bearing capacity of beams at mid-span under the baseline travelling fire scenario. According to Eurocode 3, the degree of utilisation is used for the ultimate limit state design of uniform steel beam with I-section [53]. The corresponding design resistance in the fire situation, i.e. $N_{fi,Rd}$ for tension or compression, and $M_{fi,Rd}$ for bending, was adopted to conservatively evaluate the beam utilisation, as shown in Fig. 10. Moreover, the effective yield strength of steel at elevated temperature θ_a was adopted, and the temperature of steel θ_a is defined according to the maximum temperature through the member section depth. By comparing Fig. 9 and Fig. 10, it is observed that considering the corresponding design resistance in the fire situation with the effective yield strength at elevated temperature θ_a, the evaluation results of beam load-bearing capacity are more conservative, especially during the heating phase.

As part of the performance-based structural fire design, in addition to determining the load-bearing capacity, the analysis of the stress state is also an important criteria. Based upon the leading author's work experience at Arup Shanghai, to assess the fire resistance performance of the complex large-span structures in practical projects (e.g. Beijing Daxing International Airport [64]), the structural stress state (i.e. Von Mises stress) analysis coupled with the structural deformation/plastic deformation analysis were adopted. Accordingly, by comparing Fig. 10 and Fig. 11, the utilisation of stress is usually greater than the utilisation of axial force and bending moment in the entire cross-section. Therefore, combining the definition of load-bearing capacity in Eurocode 3 and practical design experience, the stress utilisation at the mid-span of the beam is defined as one of the failure criteria of a single element in this paper, i.e. the ratio of the axial stress envelope in the whole beam cross-section over the steel yield strength, as shown in Fig. 9. The failure is defined as the beam reaches its yield capacity and can no longer support the structure above [63], i.e. the stress utilisation reaches 1.0 in this study. Furthermore, we also examined the baseline scenario where the stress utilisation that considers the temperature-dependent steel yield strength over the section will be conservative or non-conservative when compared to the steel yield strength at ambient temperature (i.e. 355 MPa at 20 °C). According to the comparison between Fig. 11(a) and Fig. 11(b), the effect of the reduction of steel strength in elevated temperature is not significant on the stress utilisation of the beam. This may be related to the stress state on the cross-section when the beam is heated. At the lower flange, the bending moment due to deflection and the compressive stress induced by the restrained thermal expansion were effectively cancelled out by each other. In contrast, at the upper flange, the effects of bending moment and the compressive force were superimposed. However, during the heating phase, the temperature-dependent steel yield strength decreased obviously in the lower flange and web, but the effect of heating on the upper flange was less significant. Based on the above reasons, the stress utilisation considering the steel yield strength at ambient temperature (i.e. 355 MPa at 20 °C) is conservative enough to be adopted as the failure criterion.

The investigation of the prototype structure under the baseline travelling fire scenario implies that, in the performance-based structural design practice, solely estimating one criterion (e.g. critical temperature) might be over-conservative. The structural responses, including deflection and the utilisation of beams should also be considered to

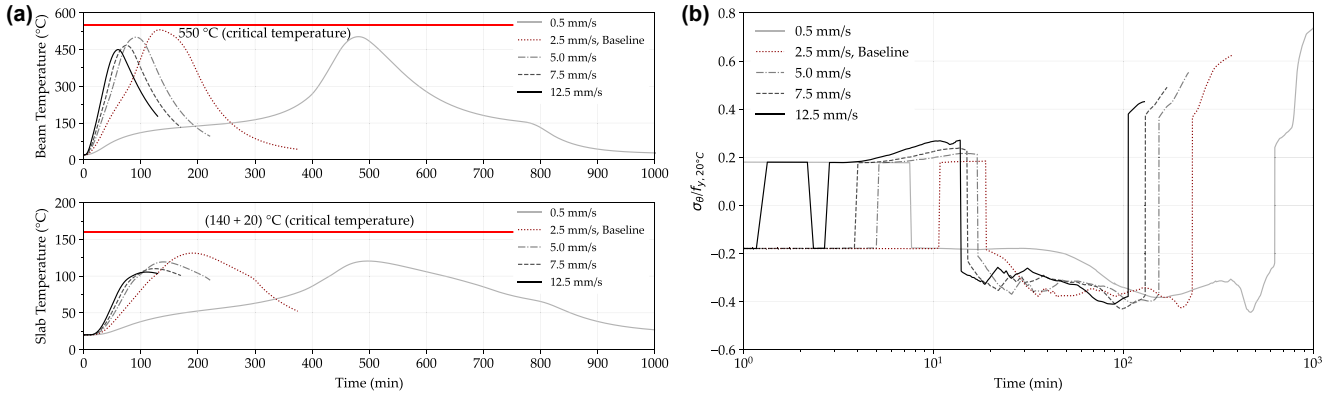

Fig. 12. Temperature and axial stress development under various travelling fire spread rates - 0.5 mm/s, 2.5 mm/s (baseline), 5.0 mm/s, 7.5 mm/s, and 12.5 mm/s on: (a). Beam6 bottom flange and Slab5 top surface temperatures; and (b). Ratio of the axial stress envelope in the Beam6 mid-span section over the yield strength 355 MPa at 20 °C.

guarantee a sufficient and economic design.

4. Travelling fire scenario

The structural response under the ETFM framework with various fire-related input parameters is presented in this section. It includes travelling fire spread rate, fire load density, and inverse opening factor (IOF).

4.1. Travelling fire spread rates

Travelling fire spread rates are among the most important design parameters for the thermal analysis of the structural members in a large compartment [22,70], however, their structural impact is still unclear, though pioneering work had been carried out [19,23,38–40], especially while the structural elements are supplied with fire protection to meet the required FRR (e.g. one hour rating in the baseline scenario) and the concrete slab is carrying the majority of the loading at high temperature. The selection of the travelling fire spread rates followed the literature summary by Dai et al. in 2020 [22], i.e. 0.5 mm/s, 2.5 mm/s (baseline), 5.0 mm/s, 7.5 mm/s, and 12.5 mm/s. The purpose of this section is to investigate the effect of different travelling fire spread rates on the thermal and structural responses of the prototype structure with composite floors.

Fig. 12(a) presents the thermal response of the steel Beam6 bottom flange and concrete Slab5 top surface, respectively, under the selected travelling fire spread rates. Beam6 and Slab5 were both at the second bay, which tends to have the largest structural deflections according to the findings in the aforementioned baseline travelling fire scenario. All the setup of the design travelling fire parameters were kept the same as the baseline scenario, except for changing the fire spread rates. The thermal impact of the fire spread rates on the protected steel members' bottom flange, as well as on the concrete slabs' top surface, were not distinguishable on their peak temperatures (i.e. 450 °C to 530 °C for the steel members, 85 °C to 105 °C for the concrete slabs). Instead, their predominant impact was mainly reflected in the total duration of one heat-cooling cycle, which was inversely proportional to their corresponding fire spread rates. The "non-distinguishable" peak member temperatures are mainly due to the "combination effect" of the presence of fire protection/concrete slab, and the travelling fire spread rate. When a fast travelling fire (e.g. 12.5 mm/s) approaches a structural member with a very high resultant HRR [22], i.e. 38 MW, it will also rapidly

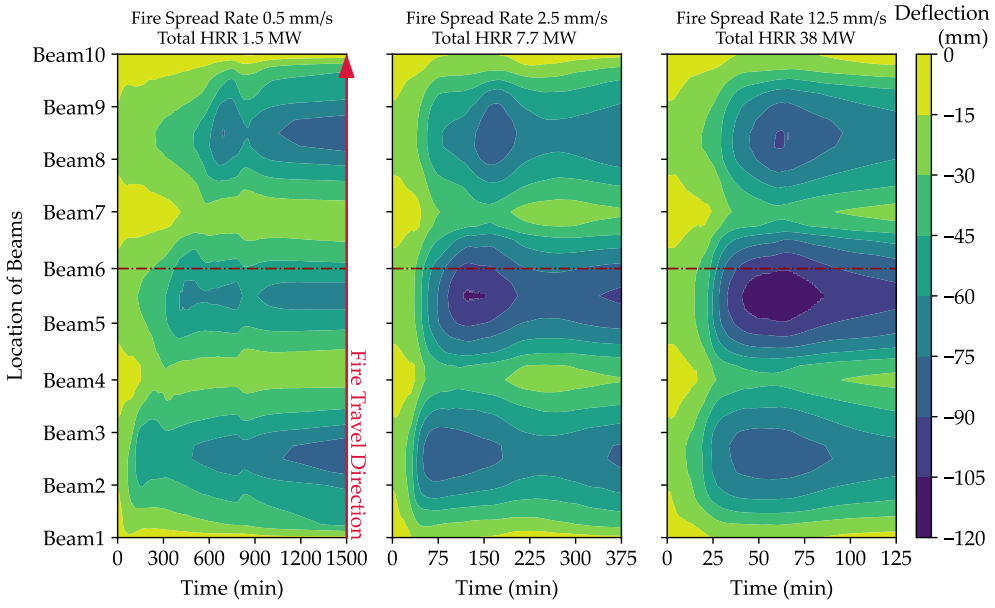

Fig. 13. Contour of deflection at mid-span of the composite floor (all beams and slabs) under various travelling fire spread rates, 0.5 mm/s, 2.5 mm/s (baseline), and 12.5 mm/s.

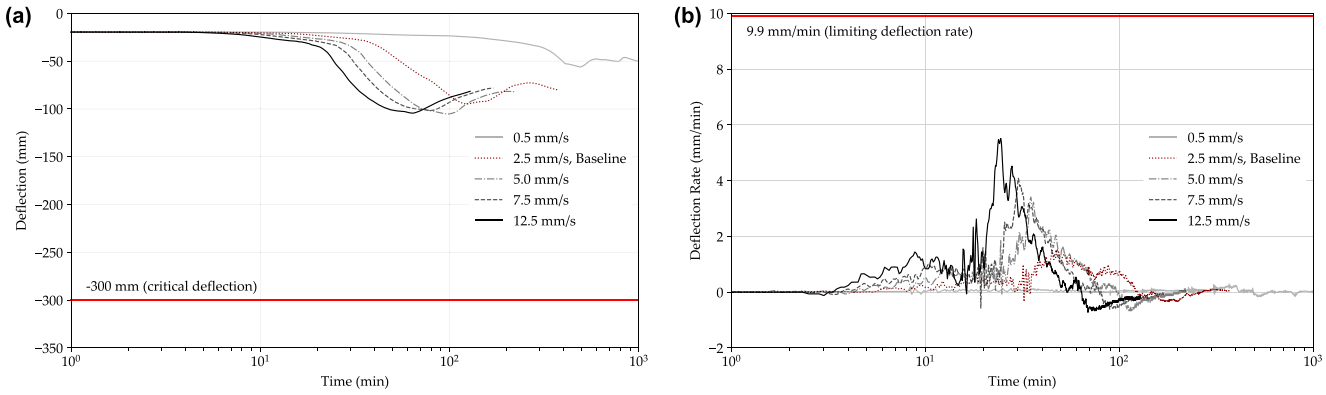

Fig. 14. Deflection of Beam6 at mid-span under various travelling fire spread rates, 0.5 mm/s, 2.5 mm/s (baseline), 5.0 mm/s, 7.5 mm/s, and 12.5 mm/s: (a). Deflection; and (b). Deflection rate.

move away from the structural member, reducing the total near field exposure time for that member. By contrast, when a slow travelling fire (e.g. 0.5 mm/s) approaches a structural member even with a modest total HRR, i.e. 1.5 MW, the longer near field exposure will provide the fire a lot more time to "heat up" the structural member, which may result in more energy being absorbed by the structural member. As shown in Fig. 12(b), the stress utilisation of the steel Beam6 reached 0.43 and 0.75 for the travelling fires with fire spread rates 12.5 mm/s and 0.5 mm/s respectively, due to the increasing tensile stresses during the cooling phase. Meanwhile, as shown in Fig. 13, the residual deflections also increased under travelling fire scenarios with lower fire spread rates (i.e. 0.5 mm/s and 2.5 mm/s) during the cooling phase. This further implies that "slow" travelling fires cannot be ignored in performance-based structural design.

Fig. 13 demonstrates the structural deflections along the travelling fire trajectory, from Beam1 to Beam10, as time evolves. Among the three cases with fire spread rates of 0.5 mm/s, 2.5 mm/s (baseline), and 12.5 mm/s, it was found that 12.5 mm/s resulted in the largest structural deflection in the concrete slab between Beam5 and Beam6, i.e. Slab5. However, the structural deflections at mid-span under 2.5 mm/s fire spread rate scenario were similar to the structural deflections under 12.5 mm/s fire spread rate scenario, even though the resultant HRR of the fire scenario with 12.5 mm/s fire spread rate was five times larger than the fire scenario with 2.5 mm/s fire spread rate. Again, the reason behind this was due to the aforementioned "combination effect", between the presence of fire protection/concrete slab, and the travelling fire spread rate. An exemplar of this deflection result is presented in Fig. 14(a), that in the group of travelling fire scenarios with increasing fire spread rates 5.0 mm/s, 7.5 mm/s, and 12.5 mm/s, the maximum deflections of those cases were similar, i.e. 105 mm, 102 mm, and 104 mm, respectively. The lowest deflection was 56 mm, related to the slowest travelling fire, 0.5 mm/s, and is probably due to the fact that only a limited number of the structural elements were heated by this smaller 1.5 MW fire. This fire could only impact a limited area of the structure while the remainder of the structural bays stay at a relatively low temperature, and still provide high stiffness and load redistribution paths to prevent the heated part of the structure from deflecting significantly. Further, the presence of the concrete slab increases the continuity of the whole structure, compared to a 2D steel framed structural analysis. More detailed 2D vs 3D modelling under the travelling fires on the interpretation of the structural response is discussed in Section 7.1. Fig. 14(b) illustrates the deflection rates of Beam6, showing that fire spread rates have a limited impact on this value.

4.2. Fuel load densities

In the ETFM framework, it is assumed that all fuel load would be consumed over the entire fire duration [22]. Hence, the resultant HRR and the fire duration of travelling fire scenarios are directly decided by the fire spread rate and fuel load density, although the former is capped with a limit value once the fire is under entertainment-controlled burning. In the previous research by Dai et al. in 2020 [22], the fuel load density has a stronger impact than fire spread rate under certain fire scenario combinations. In this section, the investigated fuel load densities according to Eurocode 1 [59] considering 80 % fractile are: 280 MJ/m^2 (hospital room), 365 MJ/m^2 (theatre cinema), 511 MJ/m^2 (baseline) (office), and 730 MJ/m^2 (shopping centre). It aims to investigate the effect of different characteristic fuel loads for the structural

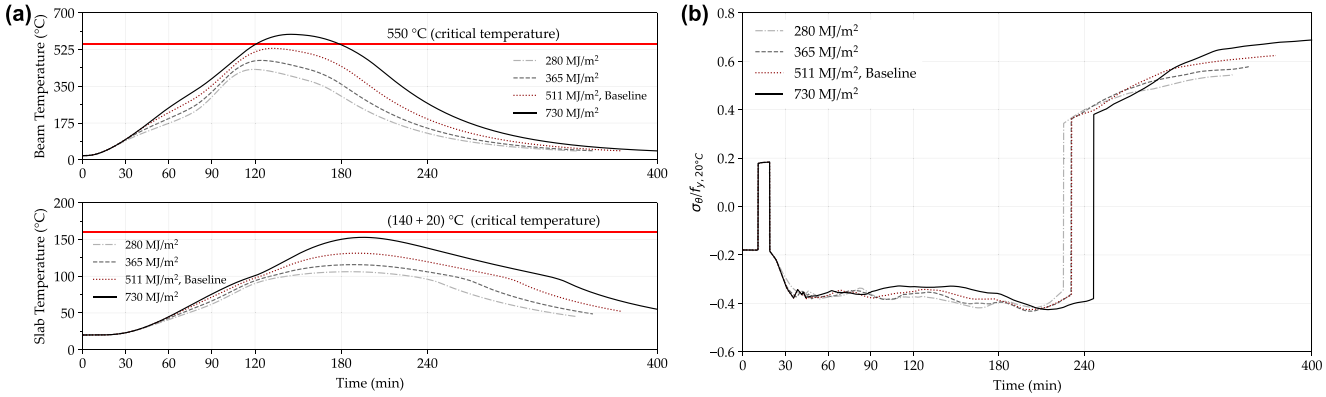

Fig. 15. Temperature and axial stress development under different fuel load densities, 280 MJ/m^2, 365 MJ/m^2, 511 MJ/m^2 (baseline), and 730 MJ/m^2 on: (a). Beam6 bottom flange and Slab5 top surface temperatures; and (b). Ratio of the axial stress envelope in the Beam6 mid-span section over the yield strength 355 MPa at 20 °C.

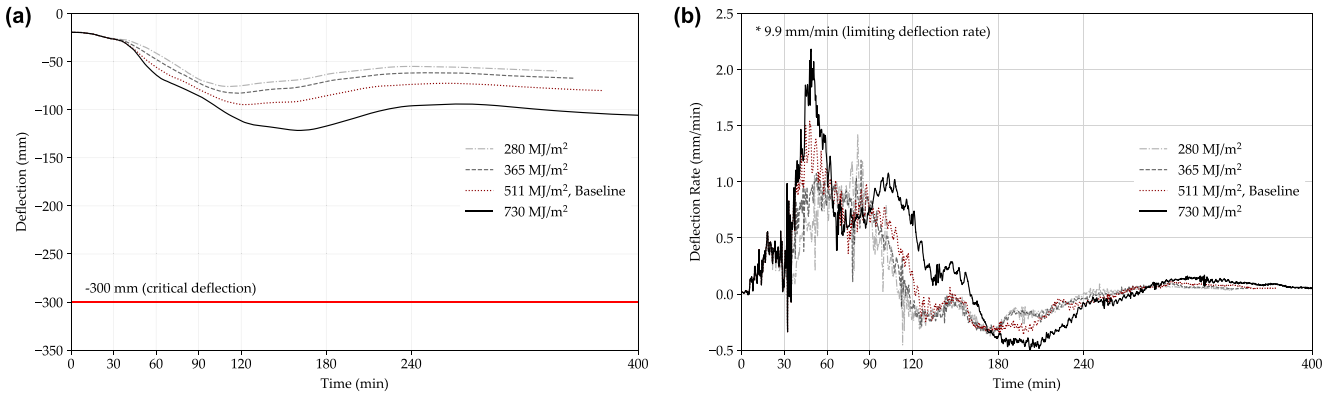

Fig. 16. Deflection of Beam6 at mid-span under different fuel load densities, 280 MJ/m^2, 365 MJ/m^2, 511 MJ/m^2 (baseline), and 730 MJ/m^2: (a). Deflection; and (b). Deflection rate.

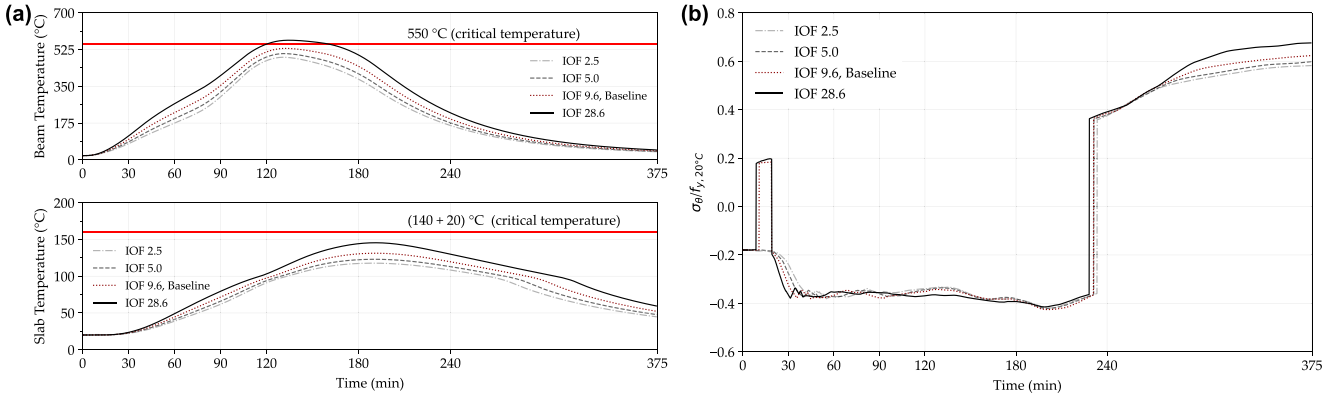

Fig. 17. Temperature and axial stress development with different IOF, 2.5, 5.0, 9.6 (baseline), and 28.6 on: (a). Beam6 bottom flange and Slab5 top surface temperatures; and (b). Ratio of the axial stress envelope in the Beam6 mid-span section over the yield strength 355 MPa at 20 °C.

response, while retaining the values of all other parameters the same as the baseline scenario.

As shown in Fig. 15(a), with increasing fuel load densities, 280 MJ/m^2, 365 MJ/m^2, 511 MJ/m^2 (baseline), and 730 MJ/m^2, the peak temperature of Beam6 at mid-span was also increasing to 430 °C, 473 °C, 531 °C, and 598 °C, respectively. Fig. 15(a) also shows the time to reach maximum temperature of the steel Beam6 ranging from 106 min to 152 min, which is proportional to their corresponding fuel load densities. The sudden change in stress utilisation of Beam6 also occurred at different times (i.e. from compression in the heating phase to tension in the cooling phase), as shown in Fig. 15(b). This is due to, in the ETFM framework, the burn-out time being introduced to quantify the time needed for burning out a certain area of fuel completely [22], which is proportional to fuel load densities. When the fuel load density was high enough (i.e. 730 MJ/m^2), the peak temperature of Beam6 exceeded the critical temperature of the steel beam (i.e. 550 °C) and reached 598 °C, while the peak temperature of Slab5 top surface reached 153 °C which is close to the critical temperature of the concrete slab (i.e. 160 °C).

As shown in Fig. 16(a), in the group of travelling fire scenarios with increasing fuel load densities, 280 MJ/m^2, 365 MJ/m^2, 511 MJ/m^2, and 730 MJ/m^2, the maximum deflections of the Beam6 were increased, i.e. 76 mm, 83 mm, 95 mm and 122 mm, respectively. Fig. 16(b) illustrates the deflection rates of the Beam6, when the fuel load density was high enough (i.e. 730 MJ/m^2), the deflection rate of the steel beams increased

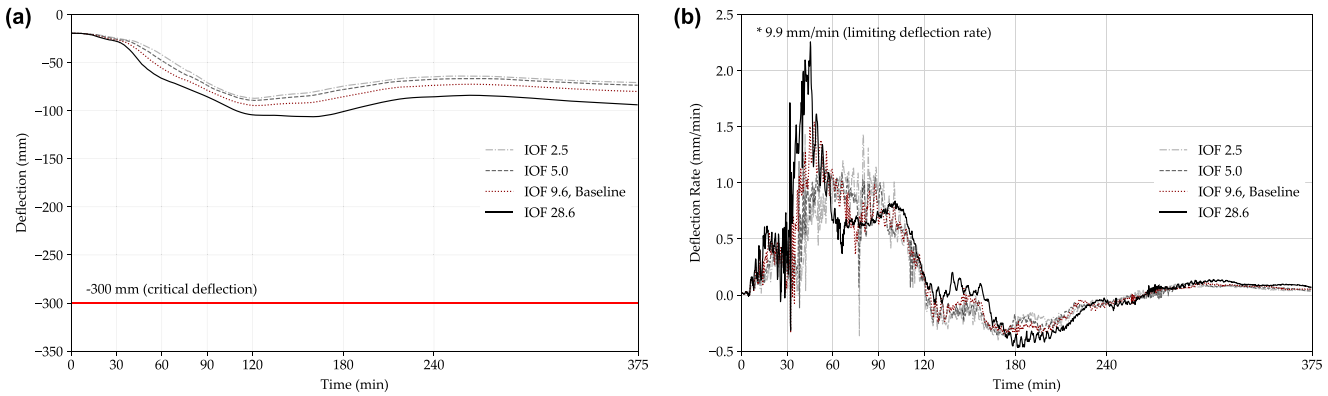

Fig. 18. Deflection of Beam6 at mid-span with different IOF, 2.5, 5.0, 9.6 (baseline), and 28.6: (a). Deflection; and (b). Deflection rate.

Table 1
Summary of the case studies for the thermal and structural response and corresponding failure criteria, under various travelling fire scenarios (values in bold for highlighting failure, or very close to failure).

Case No.	Fire spread rate (mm/s)	Fuel load density (MJ/m^2)	Inverse opening factor (IOF)	Total HRR (MW)	Critical temperature (°C)		Critical deflection L/20 (mm)		Stress utilisation $\sigma_0/f_{y,20\,°C}$	
					Beam (550)	Slab unexposed (140+20)	Beam (−8300)	Slab (−300)	Beam yield stress (355MPa)	
									Tension	Compression
1*	2.5	511	9.6	7.67	***549***	133	−95	−107	0.63	−0.53
2	0.5	511	9.6	1.53	503	121	−71	−90	***0.93***	−0.60
3	5.0	511	9.6	15.33	531	122	−105	−120	0.57	−0.56
4	7.5	511	9.6	23.00	492	112	−103	−116	0.52	−0.55
5	12.5	511	9.6	38.33	450	106	−104	−118	0.46	−0.54
6	2.5	280	9.6	4.20	443	107	−76	−87	0.54	−0.54
7	2.5	365	9.6	5.48	488	117	−83	−93	0.58	−0.53
8	2.5	730	9.6	10.95	***619***	***158***	−122	−135	0.69	−0.53
9	2.5	511	2.5	7.67	504	119	−87	−99	0.58	−0.54
10	2.5	511	5.0	7.67	523	124	−89	−102	0.60	−0.54
11	2.5	511	28.6	7.67	***589***	148	−106	−120	0.68	−0.52

* Case 1 is the baseline scenario.

significantly in the heating phase. Again, as the fuel load density is higher, it would generate larger HRR and longer heating duration correspondingly, and the localised heating domination by the near-field fire would be more significant.

4.3. Opening factors

Another important travelling fire design parameter which might affect the structural response is the inverse opening factor (IOF) [22], which has a direct impact on the accumulated smoke temperature for preheating the structural elements at the far-field in the large compartment. The IOF is changed by modifying the large compartment window soffit height (see Fig. 6(a)), resulting in equivalent IOF of 2.5, 5.0, 9.6 (baseline), and 28.6 accordingly (i.e., with decreasing opening size), while maintaining the values of all other parameters the same as the baseline scenario.

Unlike the structural response sensitivities due to various travelling fire spread rates and fuel load densities, the impact of the opening factor is not significant and displays a very linear relationship with the resultant thermal and structural response of the structural members, as presented in Fig. 17 and Fig. 18. For example, with increasing IOF (i.e. decreasing opening size), 2.5, 5.0, 9.6 (baseline), and 28.6, the maximum steel member bottom flange temperatures are also increasing, to 480 °C, 500 °C, 525 °C, and 575 °C, respectively. This is due to more energy being confined within the large compartment as the opening size is reduced, hence higher gas phase temperatures are predicted by the ETFM framework. It is worth noting that higher gas phase temperatures due to reducing opening sizes also increase the stress utilisation of beams in the cooling phase as shown in Fig. 17(b). For example, with increasing IOF (i.e. decreasing opening size), 2.5, 5.0, 9.6 (baseline), and 28.6, the maximum utilisation of Beam6 at mid-span is also increasing, as 0.58, 0.59, 0.62, and 0.68, respectively.

4.4. Analysis of parametric studies

This parametric study assessed the structural fire performance under various travelling fire scenarios considering different failure criteria. As shown in Table 1, a single criterion cannot ensure a safe structural design under travelling fires: 1) under different fire spread rates, the failure of structural steel beams for case 1 and 2, were determined according to the critical temperature (i.e. 550 °C) and the stress utilisation (i.e. reaching to 1), respectively. The failure case 2 caused by the large tensile axial force during the cooling phase implied that the slow travelling fires are also necessary travelling fire scenarios to be considered in design. Due to the "combination effect" of the presence of fire protection/concrete slab and the travelling fire spread rate, the difference of deflection and stress utilisation is relevantly small for "fast" travelling fires, e.g., 5.0 mm/s, 7.5 mm/s and 12.5 mm/s; 2) under different fuel load densities, the failure of structural elements occurs for case 1 and 8 were determined by the critical temperature. The structural element peak temperatures, deflections and stress utilisation of beams under compression all increased with increasing fuel load densities; 3) under different IOF, the failure of structural steel beams for case 1 and 11 were also determined by the critical temperature. Although the IOF has a limited impact on the structural responses, the IOF still directly affects the smoke layer (thickness and temperature of the far-field accumulated

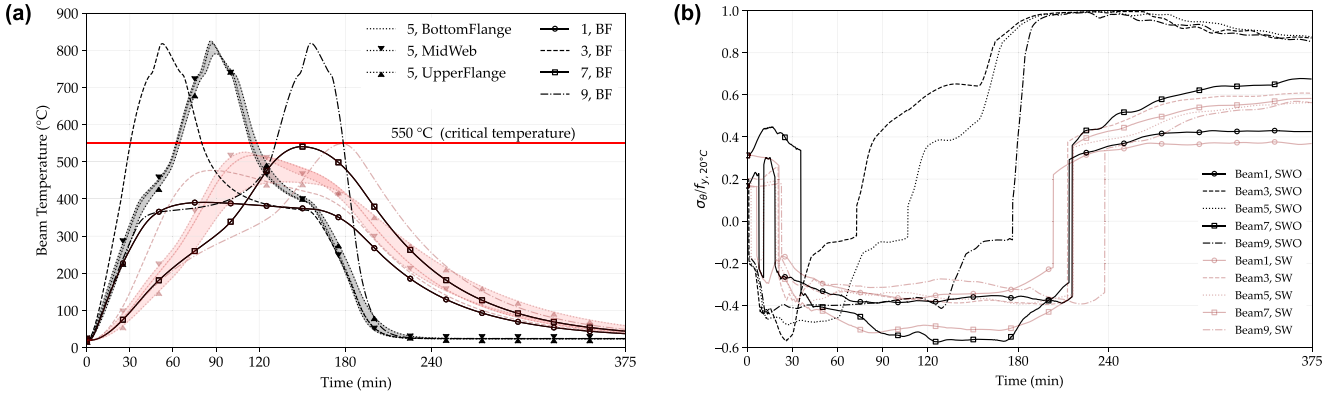

Fig. 19. Thermal and mechanical response at mid-span of the beams under the baseline travelling fire scenario with different fire protection schemes, **SWO** and **SW**: (a). Temperature development; and (b). Ratio of the axial stress envelope in the beams section over the yield strength 355 MPa at 20 °C.

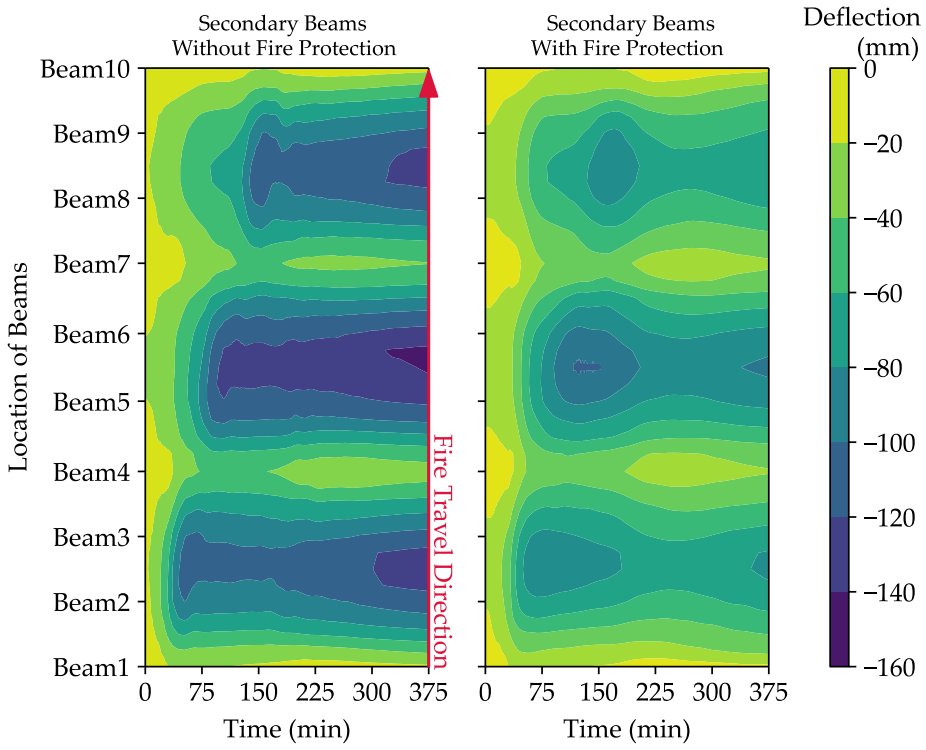

Fig. 20. Contour of deflection at mid-span of the composite floor (all beams and slabs) under the baseline travelling fire scenario with different fire protection schemes.

smoke layer), and has a direct impact on the heating and cooling phases. To summarise, it is recommended while applying the travelling fires for structural design, various travelling fire scenarios should be considered.

5. Fire protection

5.1. Fire protection scheme: with/without secondary beam fire protection

Fire protection is one of the related structural design parameters which has a significant effect on the fire resistance of structures. It is recognized that columns and primary beams are usually protected in practice [65]. For conventional fire resistance design, the general approach is to protect all structural steel members to achieve the required FRR. However, for performance-based design of steel-composite floor systems, an alternative is to protect the columns and primary beams only and leave the secondary beams unprotected, to further encourage the development of the tensile membrane action (TMA) [66–69]. This section investigates the effect of fire protection removal of the secondary beams on the thermal-mechanical responses of the prototype structure with the composite floor under travelling fires. Note that all beams and columns were protected in the previous baseline travelling fire scenario with one-hour FRR. Two fire protection schemes were carried out:

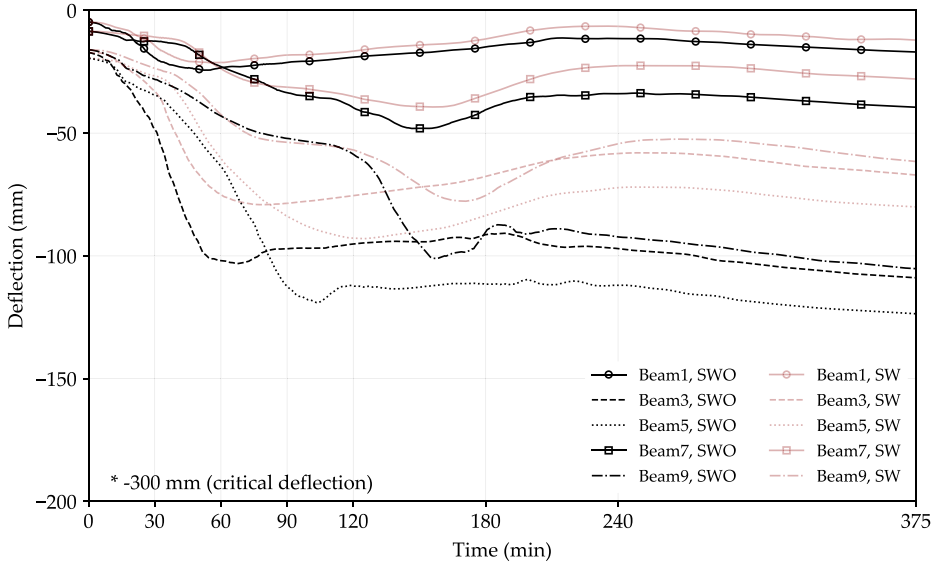

Fig. 21. Deflection of the beams at mid-span under the baseline travelling fire scenario with different fire protection schemes: **SWO** and **SW**.

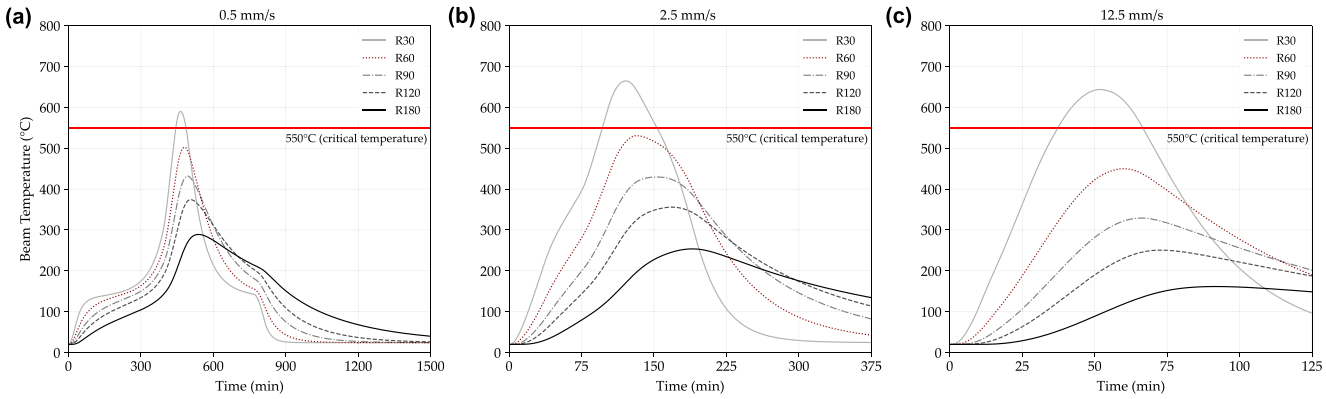

Fig. 22. Temperature development of the Beam6 bottom flange with different FRR - R30, R60, R90, R120 and R180 under various travelling fire spread rates: (a). 0.5 mm/s; (b). 2.5 mm/s; and (c). 12.5 mm/s.

- **SW** - the columns and primary beams are protected, **with** fire protection of the **s**econdary beams (referring to the prototype structure under the baseline travelling fire scenario in Section 3).
- **SWO** - the columns and primary beams are protected, **without** fire protection of the **s**econdary beams.

Fig. 19(a) presents thermal response at mid-span of the steel beams under the baseline travelling fire scenario with different fire protection schemes. Due to the effect of fire protection, the peak temperature of the secondary beams dropped 33 %, i.e. from 820 °C to 550 °C, and formed a more clear thermal gradient in the beam section depth. Fig. 19(b) presents the comparison of stress utilisation between the two fire protection schemes, i.e. SWO and SW. As shown in Fig. 19(b), stress utilisation of unprotected secondary beams reached 1.0. This was caused by the larger tensile stresses increasing in the cooling phase. Meanwhile, Fig. 19(b) also shows that the removal of the fire protection of secondary beams (i.e. SWO) has a limited impact on the stress utilisation of the primary beams, though the secondary beams have failed. This is due to the presence of the slabs, these carrying more loads after the failure of secondary beams. As shown in Fig. 20, the deflection also increased obviously when the SWO fire protection scheme was adopted. This further implies that leaving the secondary beams unprotected encourages the development of the tensile membrane action under travelling fires, which may enhance the fire resistance of the whole structure.

According to the deflections shown in Fig. 20 and Fig. 21, although the secondary beams failed in terms of the stress utilisation, the peak deflection increased 38 %, i.e. the deflection of Beam3 increased from 79 mm to 109 mm for the SW and SWO respectively, which is still much smaller than the critical deflection (i.e. 300 mm). This implies that the SWO approach (i.e. secondary beams without fire protection) is also an acceptable alternative for optimizing fire protection of a structure with the composite floor, even under the travelling fire scenarios.

5.2. *Combined effect of fire protection and travelling fire spread rates*

In literature, Jiang and Li [44] analysed the effects of fire protection on collapse modes and load redistribution schemes of 3D steel-frame structures exposed to compartment fires. It was found that the whole structure may have a higher FRR than individual members due to integrity, and fire protection of steel members plays an important role to prevent fire-induced disproportionate collapses. In this study, the thickness of the mineral fibre spray (i.e. fire protection) required to deliver the equivalent FRR for structural components was based on the simplified calculation in Eurocode 3 [53]. Hence, the parametric studies on various combinations of fire protection (i.e. equivalent FRR) and travelling fire spread rates were conducted. Beams were designed with five commonly adopted FRR according to the Eurocode 4 [75] (i.e. R30, R60, R90, R120, and R180) under the investigated travelling fire scenarios with different travelling fire spread rates (i.e. 0.5 mm/s, 2.5 mm/s, and 12.5 mm/s). Here, the general approach of fire protection was adopted (i.e. **SW**). For columns, the temperature reduction ratio 0.7 was applied through column height to achieve a higher FRR.

Fig. 22 presents the thermal response at mid-span of Beam6 under 15 different combination scenarios. When fire protection was lower (i.e. R30), the peak temperature of Beam6 exceeded the critical temperature of 550 °C. With higher FRR, the peak temperature of steel beams was decreased and the occurrence of peak temperature was delayed. For instance, under the travelling fire scenario with fire spread rate 0.5 mm/s, the peak temperature of Beam6 decreased from 590 °C (R30) to 280 °C (R180), the peak temperature dropped 75 °C and the occurrence of the peak temperature was delayed 19 min on average; under the travelling fire scenario with fire spread rate 12.5 mm/s, the peak temperature of Beam6 decreased from 644 °C (R30) to 162 °C (R180), the peak temperature drops 121 °C and the occurrence of the peak temperature was delayed 10 min on average. Hence, under travelling fire scenarios, considering different fire spread rates, the effect of fire protection on thermal responses of the steel beams is different. When a slow travelling fire (e.g. 0.5 mm/s) approaches a structural member with a modest total HRR, i.e. 1.5 MW, the occurrence of the peak temperature of steel beams can be delayed effectively by increasing FRR. When a fast travelling fire (e.g. 12.5 mm/s) approaches a structural member with a very high total HRR, i.e. 38MW, the peak temperature of steel beams can be decreased effectively by increasing FRR. The reason behind this is due to the combined effect of FRR and travelling fire spread rates. The external heat for steel beams is mainly affected by size and the "stay" duration of the localised burning, and note that fire size is proportional to the fire spread rate.

Fig. 23 presents the deflection of the structure under various travelling fire spread rates with different FRR of steel beams. Under the travelling fire scenario with spread rate 0.5 mm/s, the effect of increasing FRR on deflection of the structure was insignificant. The maximum deflection of the structure only decreased 19 mm, from 99 mm (R30) to 80 mm (R180). When travelling fire spread rates increase, the effect of increasing FRR on the deflection of the structure becomes more significant. For example, with increasing FRR (from R30 to R180), under the travelling fire scenario with fire spread rate 2.5 mm/s, the deflection decreased 46 %, from 157 mm (R30) to 85 mm (R180); under the travelling fire scenario with spread rate 12.5 mm/s, the deflection decreased 72 %, from 183 mm (R30) to 52 mm (R180). The global structural responses under the travelling fire scenario with travelling fire spread rate 0.5 mm/s are different from the other two travelling fire spread rates. As shown in Fig. 23, the maximum deflection always occurred in the "side" bays (i.e. BAY 1 and BAY 3 as described in Fig. 5 (b)) under the travelling fire scenario with spread rate 0.5 mm/s. Again, this is due to the structural responses being more significantly dominant in the cooling phase, when a fire travelled slowly (e.g. 0.5 mm/s) with a

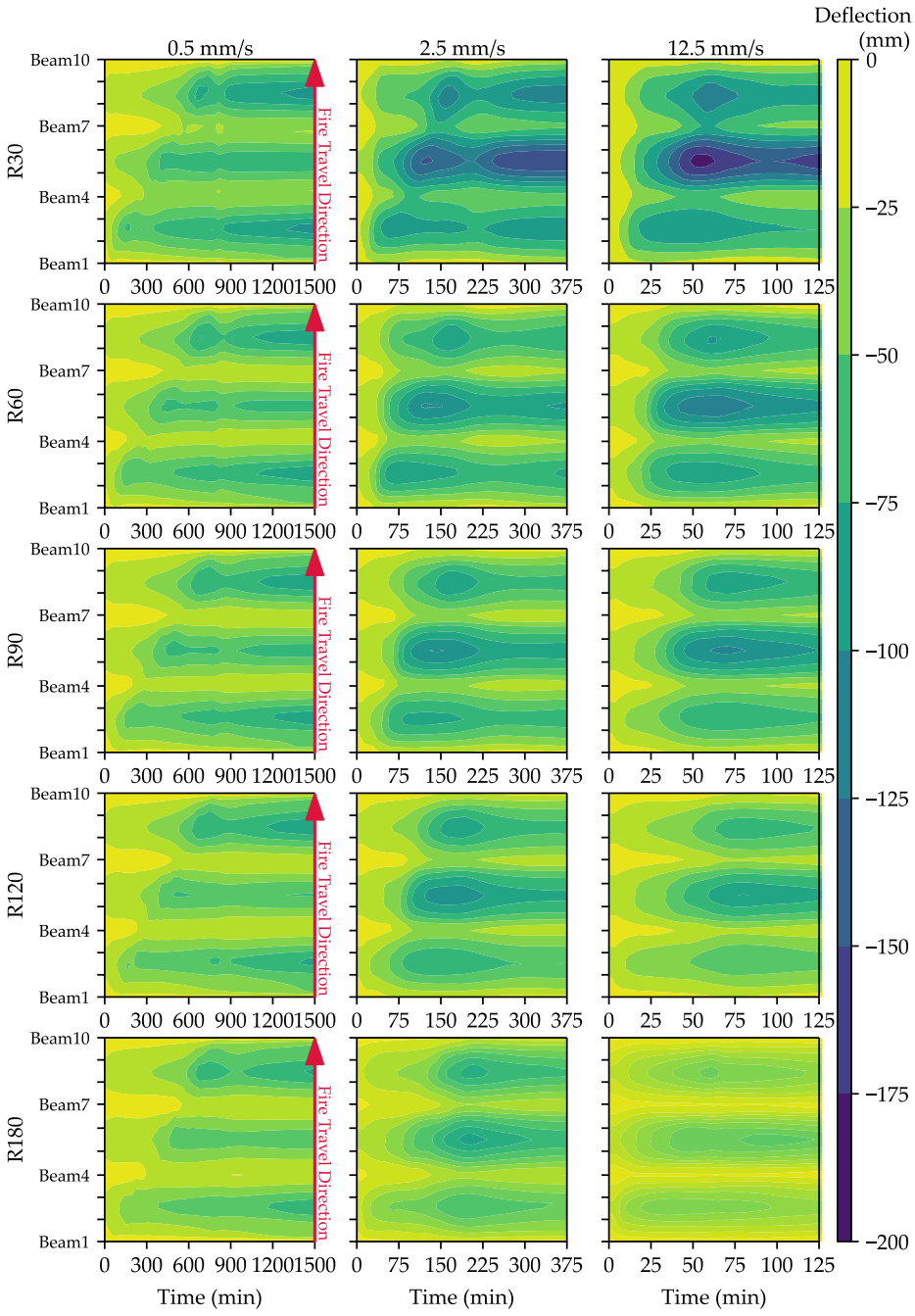

Fig. 23. Contour of deflection at mid-span of the composite floor (all beams and slabs) with different FRR of all beams - R30, R60, R90, R120 and R180 under various travelling fire spread rates - 0.5 mm/s, 2.5 mm/s and 12.5 mm/s.

modest total HRR, i.e. 1.5 MW. Under the travelling fire scenarios with higher spread rates 2.5 mm/s and 12.5 mm/s, the largest deflection occurred in BAY2 with a longer span (i.e. 8 m) instead of the "side" bays. Hence, the global structural response, or the potential structural failure mechanism (if the load ratio was being artificially increased until the structure collapsed, Jiang et al. [49]), might be also affected by the layout of the structure, in combination with the FRR and the fire spread rate simultaneously.

Fig. 24 summarises the maximum stress utilisation at mid-span with different FRR of all beams (i.e. R30, R60, R90, R120 and R180) under various travelling fire spread rates (i.e. 0.5 mm/s, 2.5 mm/s and 12.5 mm/s). In Fig. 24(a), given the steel beams under compression, the changes of travelling fire spread rate or FRR have little effect on the stress utilisation of the steel beams which are between 0.2 and 0.6. In Fig. 24(b), given the steel beams under tension, with travelling fire spread rate 0.5 mm/s, the stress utilisation of steel beams decreased effectively with increasing FRR. However, with travelling fire spread rates 2.5 mm/s and 12.5 mm/s, when the FRR exceeded a certain level, the tension stress utilisation of steel beams increased with increasing FRR. This is due to the fact that the internal force of steel beams under fire is mainly affected by two types of deformation. The thermal expansion leading the steel beams to undergo compression, and the deflection reducing the compressive force, may cause the steel beams to undergo bending. The thermal expansion and deflection interact on the section and dominate in different phases. In addition, steel beams experience tension during the cooling phase or when the steel material softens due to high temperatures.

When the steel beams were heated at a relatively higher temperature,

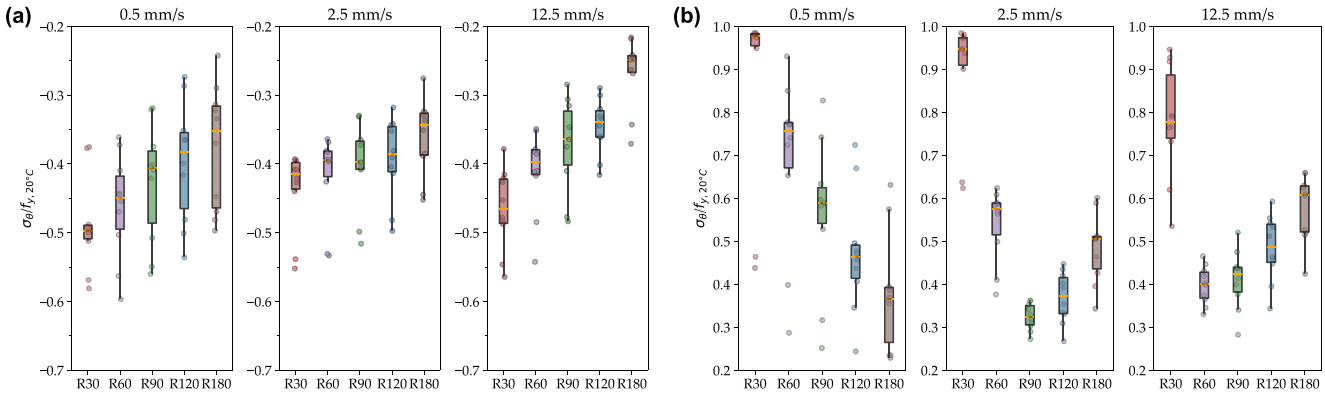

Fig. 24. Maximum stress utilisation at mid-span with different FRR of all beams - R30, R60, R90, R120 and R180 under various travelling fire spread rates - 0.5 mm/s, 2.5 mm/s and 12.5 mm/s: (a). Compression; and (b). Tension.

the compression and bending by the thermal expansion dominated the internal force analysis. In this phase, the utilisation of compression stress was reduced by enhancing fire protection (see Fig. 24(a)). For instance, under the travelling fire scenario with fire spread rate 0.5 mm/s, the median of compression stress utilisation decreased from 0.50 (R30) to 0.35 (R180); under the travelling fire scenario with fire spread rate 12.5 mm/s, the median of compression stress utilisation decreased from 0.46 (R30) to 0.25 (R180). Note that the effect of enhancing fire protection on the compression stress utilisation is not significant for the travelling fire scenario with spread rate 2.5 mm/s. This is due to the interaction between fire size and "stay" duration of localised burning.

When the steel beams with a relatively lower temperature, i.e. the fire protection is "thick" enough to prevent the heating effectively, or the cooling phase, the tension and bending dominated the internal force analysis. In these phases, only for the travelling fire scenario with spread rate 0.5 mm/s, the utilisation of tension stress was reduced effectively by enhancing fire protection (see Fig. 24(b)). For instance, under the travelling fire scenario with fire spread rate 0.5 mm/s, with R30, R60, R90, R120 and R180, the average temperature change rate of steel beams reached 18 °C/min, 8 °C/min, 6 °C/min, 4.5 °C/min and 3 °C/min respectively, and the median of tension stress utilisation decreased from 0.98 (R30) to 0.37 (R180) correspondingly. This is due to the fact that when a slow travelling fire (e.g. 0.5 mm/s) approaches a structural member the steel beams are always directly exposed to fire for a longer time, which essentially allows the heat to permeate the fire protection. Besides, under the travelling fire scenario with fire spread rate 2.5 mm/s, the median of tension stress utilisation decreased from 0.95 (R30) to 0.32 (R90) but recovered to 0.51 (R180); under the travelling fire scenario with fire spread rate 12.5 mm/s, the median of tension stress utilisation decreased from 0.78 (R30) to 0.40 (R60) but recovered to 0.61 (R180). This is due to the sectional thermal gradients induced additional bending moments due to a shift in the section's effective centroid (i.e. the section's centre of stiffness) and a potential shift in plastic P-M capacity [63]. The sectional heat transfer was inhibited with increasing FRR, the tension and bending in the lower flange caused by the deflection dominated the internal force analysis. Details of stress capability at mid-span of all beams are presented in the Appendix. The combined effect of FRR and travelling fire spread rates should be considered, determining the fire severity of the structure under travelling fire scenarios.

With fire protection of R30, the peak temperature of steel beams exceeded 550 °C, and the utilisation of most steel beams exceeded 0.9 during the cooling phase, as shown in Fig. 24(b). The steel beams can be determined as a failure according to the criteria for single elements, either thermal or structural. However, as shown in Fig. 23, the deflections of steel beams were much less than the critical deflection 300 mm, the whole structure maintained stability under travelling fire scenarios with different travelling fire spread rates. This is due to the presence of the slab increasing the stiffness of the whole structure. It also revealed that the fire protection design could be optimised in the structure with the composite floor, which is discussed in the following section.

Table 2
Summary of the case studies with different fire protections (i.e. SWO and SW under various travelling fire scenarios for the thermal and structural response and corresponding failure criteria (values in bold for highlighting failure, or very close to failure).

Case No.	Fire protection scheme	Fire spread rate (mm/s)	FRR (min)	Critical temperature (°C)		Critical deflection L/20 (mm)		Stress utilisation $\sigma_\theta/f_{y,20}$ °C	
				Beam (550)	Slab unexposed (140+20)	Beam (−300)	Slab (−300)	Beam yield stress (355MPa)	
								Tension	Compression
1	SWO	2.5	R60	***819***	133	−129	−143	***1.0***	−0.61
2*	SW	2.5	R60	***549***	133	−95	−107	0.63	−0.53
3	SW	0.5	R30	***590***	121	−81	−99	***0.98***	−0.58
4	SW	0.5	R60	503	121	−71	−89	***0.93***	−0.60
5	SW	0.5	R90	433	121	−71	−89	0.83	−0.56
6	SW	0.5	R120	378	121	−72	−89	0.72	−0.54
7	SW	0.5	R180	298	121	−65	−80	0.63	−0.50
8	SW	2.5	R30	***669***	133	−138	−157	***0.98***	−0.55
9	SW	2.5	R90	450	133	−91	−106	0.36	−0.52
10	SW	2.5	R120	370	133	−87	−101	0.45	−0.50
11	SW	2.5	R180	258	133	−72	−85	0.60	−0.45
12	SW	12.5	R30	***647***	106	−165	−183	***0.95***	−0.56
13	SW	12.5	R60	450	106	−104	−118	0.47	−0.54
14	SW	12.5	R90	329	106	−94	−108	0.52	−0.48
15	SW	12.5	R120	251	106	−77	−91	0.59	−0.42
16	SW	12.5	R180	162	106	−43	−52	0.66	−0.37

* Case 2 is the baseline scenario.

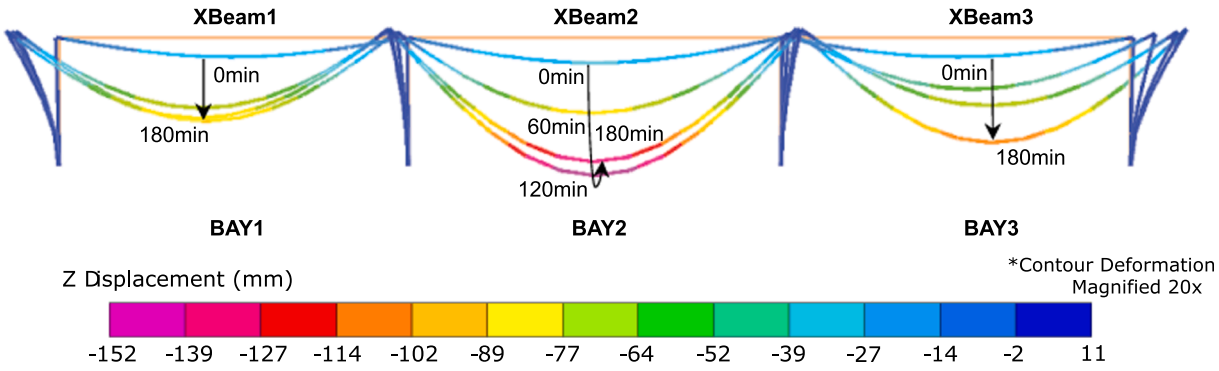

Fig. 25. Displacement contour of the 2D steel frame under the baseline travelling fire scenario with 20 times scaled.

5.3. Analysis of parametric studies

Table 2 quantifies the combined effect of fire protection (i.e. equivalent FRR) and fire spread rates on the thermal and structural response and corresponding failures. It was found that: 1) although the localised failure of beams occurred with the SWO fire protection scheme (i.e. secondary beams not protected) according to the critical temperature and stress utilisation, there was no global collapse of the structure. This revealed that the fire protection design could be optimised in the structure with the composite floor; 2) it is obvious that the beam temperature would decrease with increasing fire protection, however, the effect of increased fire protection on the structural responses under different travelling fire scenarios with various travelling fire spread rates could be very different. It is suggested that the fire protection of the structural steel beams should be sufficiently considered to prevent failure. Meanwhile, identifying the combination of the most severe fire scenario (e.g. a "fast" travelling fire 12.5 mm/s with a very high resultant HRR 38 MW) and the conservative structural analysis (e.g. a "slow" travelling fire 0.5 mm/s with a modest total HRR 1.5 MW) should be considered in performance-based design.

6. The role of slab

6.1. The effect of slab: 2D vs 3D

This study also discusses the role of slabs for structural fire resistance in simulation predictions and design of structures. In literature, earlier studies [23,38–40] mainly focused on 2D steel frames. The nature of the travelling fires, however, is fundamentally a 3D phenomenon, and 2D structural models cannot represent the complexity of behaviours presented in realistic structures, such as the development of tensile membrane action of slabs. Hence, the effect of a concrete slab was studied in a 3D FEM model in comparison with a 2D steel-framed model under travelling fires.

The 3D model studied in this section remained the same as the prototype structure presented in Section 3.1. In the 3D model, the steel beam elements shared the same nodes with the concrete shell elements, and the offset options were used to account for composite action effects between steel beams and concrete slabs. The 2D model with three spans (7.5 m, 8.0 m, and 7.5 m) was extracted from the longitudinal direction of the 3D prototype structure, i.e. Xbeams with the longest beam span in the 3D model and columns with a height of 2.75 m, as shown in Fig. 5(b). In the 2D model, the same structural element (i.e. UB 406 × 178 × 54 with steel grade S355) and fire protection (one-hour FRR) as the 3D model were applied. To deliver a direct comparison, similarly as the 2D FEM models by [23,39,40], the concrete slab and the composite action between the beams and the slab were not taken into account in the 2D model. Nevertheless, the load from the concrete slab was still taken into account, which could have resulted in the equivalent mechanical load compared to the 3D model. The design area load imposed on the slabs and the self-weight of the concrete slabs were converted to the uniformly distributed load (UDL) imposed on the beams, and the effective width of the concrete slabs was assumed as the length of the half short span (i.e. 3 m). For instance, the dead load $G_k = 0.53 + (2.64 + 1.5) \times 3 = 12.95$

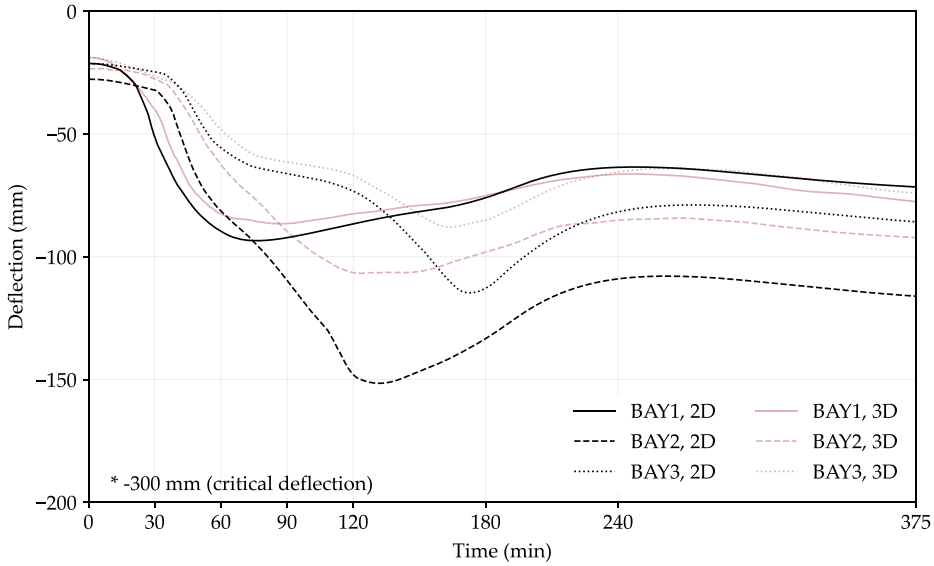

Fig. 26. Deflection at mid-span of the structural frame under the baseline travelling fire scenario: 2D model vs 3D model.

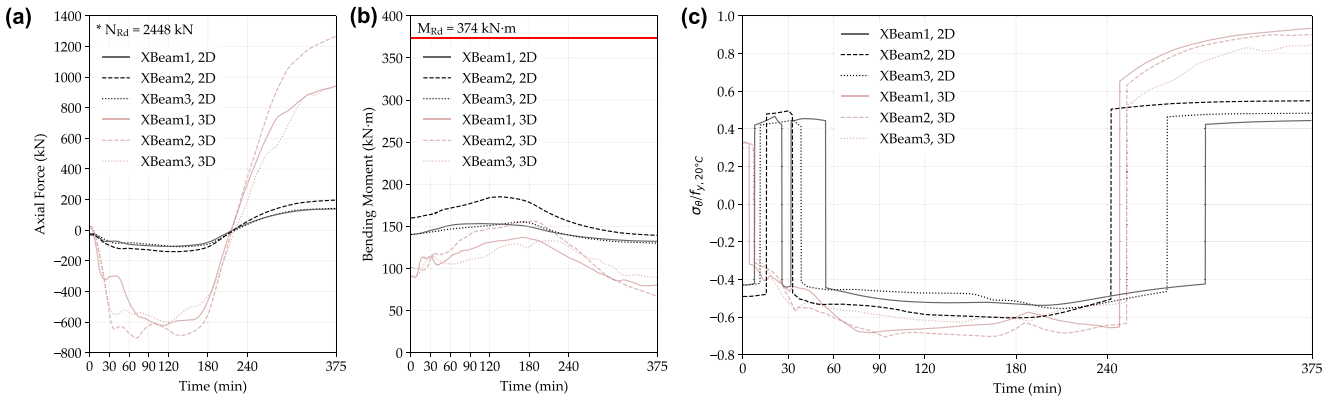

Fig. 27. Internal force and stress at mid-span under the baseline travelling fire scenario, 2D model vs 3D model: (a). Axial force; (b). Bending moment; and (c). Ratio of the axial stress envelope in the beams' mid-span section over the steel yield strength 355 Mpa at 20 °C.

kN/m and the live load $Q_k = 2.5 \times 3 = 7.5$ kN/m, were adopted as the unfactored design loads for the fire limit state, to be consistent with the 3D model. Besides, similarly as [40], the heat sink effect due to the concrete slab was considered in the heat transfer analysis of our 2D model. The travelling fire remained the same as the baseline travelling fire scenario using the ETFM framework presented in Section 3.2, for both 2D and 3D models. The fire was assumed to travel along the 2D model in the longitudinal direction to represent the equivalent fire load compared to the 3D model.

Fig. 25 presents the displacement contour of the "equivalent" 2D steel-framed structure under the baseline travelling fire scenario at every 60 mins. With comparison to Fig. 7, the structure experienced similar global structural responses in both the 3D and 2D models, with the 2D model having 27 % larger deflections on average. As shown in Fig. 26, the largest deflections of Xbeams in the 3D model were between −87 mm and −107 mm, however, the largest deflections of Xbeams in the 2D model were between −93 mm and −152 mm. This is because the 3D model has larger overall stiffness due to the presence of the concrete slab compared with the 2D model. The 2D model was observed to overestimate deflections compared to the 3D model, confirming the fundamental load-carrying role of concrete slabs at high temperatures [67–69].

Moreover, Fig. 27 presents the internal force and stress at mid-span of Xbeams under the baseline travelling fire scenario for 2D model against 3D model comparison. It is found that the structural load path mechanisms are fundamentally different between the two numerical models, i.e. with or without concrete slabs. In Fig. 27(a), all Xbeams experienced "axial force reversal" sequentially, i.e. the beams were in compression during the heating phase and in tension during the cooling phase, similarly as aforementioned in Fig. 9. However, the 3D model had more conservative values for all Xbeams. For example, in the 2D model, the maximum axial forces of Xbeams were −140 kN and 197 kN, for compression and tension respectively, which were decreased by over than 80 % compared to the 3D model. This is due to the Xbeams in the 3D model were restrained by the columns which are connected to adjacent primary beams (i.e. Zbeams) and concrete slabs, hence inducing larger axial force in the Xbeams. The more conservative values of axial force captured by the 3D model induced the connection in a more unfavorable situation, which faithfully reproduced the structural collapse under fire, namely, the collapse triggered by the failure of the connection in general, which is unlikely to be addressed in a 2D model. Fig. 27(b) shows similar force development trends between the 3D and 2D models for the bending moment of the Xbeams under the baseline travelling fire scenario, with the 2D model producing more conservative values. The realistic load redistribution cannot be captured in the 2D model as in the 3D model, where more loads were redistributed along the short span than those along the long span. Besides, the deflection of the Xbeams is induced due to the presence of the concrete slab and the adjacent structure. Hence, lower bending moments of the Xbeams were captured in the 3D model. However, as shown in Fig. 27(c), the Xbeams in the 2D model had smaller utilisation ratios under the baseline travelling fire scenario, except in the initial phase (i.e. 0 min – 60 min). During the initial phase (i.e. 0 min – 60 min), the 2D model produced the conservative utilisation ratios of Xbeams due to the rapid development of thermal expansion. These results indicate that the simplification for modelling the structure as a 2D frame is not always the most conservative under travelling fires. Besides, the running time of the 3D model using LS-DYNA was about 8 min, and the running time of the 2D model was about 3.5 min, which was only around 4 min shorter.

Considering the fundamental load-carrying role of concrete slabs at high temperatures (the more realistic load redistribution can be captured by the 3D model) and the structural collapse under fire

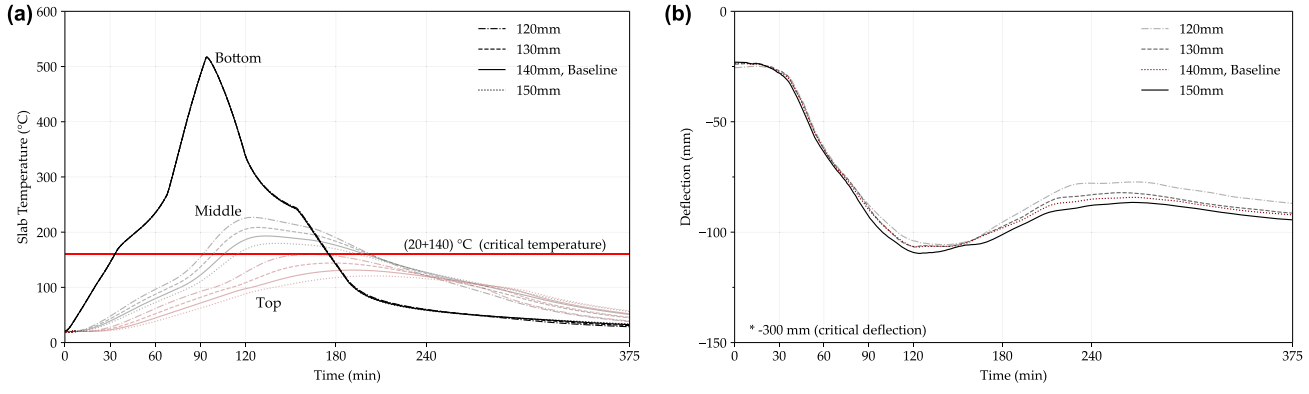

Fig. 28. Thermal and mechanical response of Slab5 at mid-span under the baseline travelling fire scenario with different slab thicknesses – 120 mm, 130 mm, 140 mm (baseline), and 150 mm: (a). Temperature development through the section; and (b). Deflection.

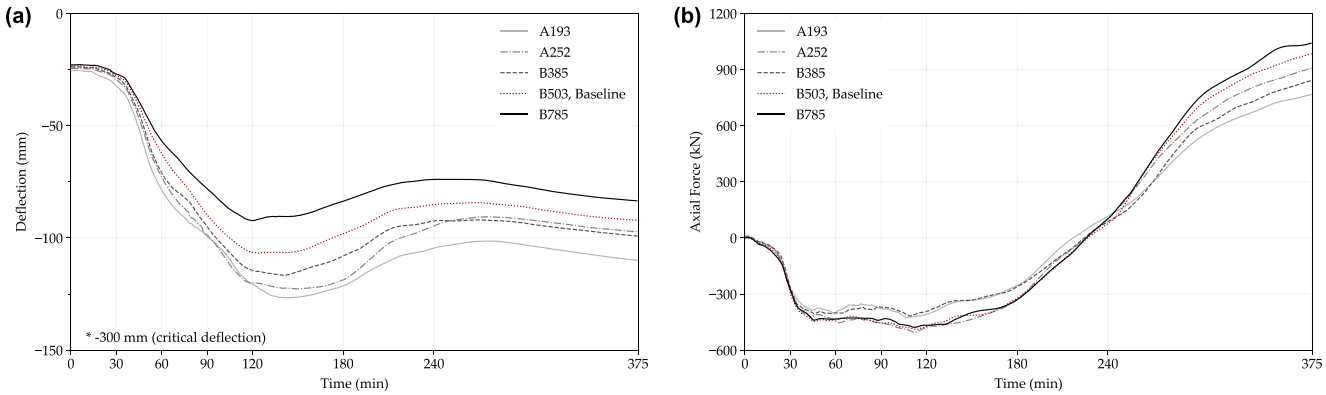

Fig. 29. Structural response of the Slab5 and Beam6 at mid-span under the baseline travelling fire scenario with different reinforcements (BS REF) - A193, A252, B385, B503 (baseline), and B785: (a). Deflection of Slab5; and (b). Axial force of Beam6.

triggered by the failure of the connection in general (the more conservative values of internal force captured by the 3D model induced the connection in a more unfavourable situation), the 3D model is necessary and feasible for structural fire analysis to consider the importance of concrete slabs under travelling fire scenarios.

6.2. Slab thicknesses and steel reinforcements

Slab thicknesses and steel reinforcements are two key parameters for the structural design of the composite floor. The effect of slab thicknesses and steel reinforcements on the global structural responses of the 3D model under the baseline travelling fire scenarios was also investigated. Different slab thicknesses were selected: 120 mm, 130 mm, 140 mm (baseline) and 150 mm, according to the Cofraplus 60 corrugated sheet for composite floors [58]. The overall steel rebar mesh A193 (i.e. 193 mm^2/1000 mm), A252 (i.e. 252 mm^2/1000 mm), B385 (i.e. 385 mm^2/1000 mm), B503 (baseline, i.e. 503 mm^2/1000 mm) and B785 (i.e. 785 mm^2/1000 mm) were selected, with the strength of 420 N/mm^2. The same simplification method used in the Veselí validation model was adopted (referring to Section 2.1). All the investigated cases are designed to meet the requirement of the one-hour fire resistance (including beams, columns and slabs) according to Eurocode 4 [75].

Fig. 28(a) presents the thermal response of Slab5 at mid-span under the baseline travelling fire scenario with different slab thicknesses, i.e. 120 mm, 130 mm, 140 mm (baseline), and 150 mm. During the heating phase, the largest peak temperature of the top surface almost reached the critical temperature, i.e. 160 °C, related to the thinnest equivalent slab thickness, i.e. 120 mm. In the group of designed slabs with increasing equivalent slab thicknesses 130 mm, 140 mm, and 150 mm, the peak temperature on the top surface was decreased, i.e. 144 °C, 131 °C and 121 °C, respectively. This is because the sectional thermal gradient increased significantly when the concrete slab thickness was increased, due to the low thermal conductivity of the concrete material. During the cooling phase, the effect of slab thicknesses on thermal response is not distinguishable. However, the impact of slab thicknesses on the deflection at mid-span of Slab5 is more significant during the cooling phase, rather than during the heating phase, as shown in Fig. 28(b). For example, with the increasing equivalent slab thicknesses, i.e. from 120 mm to 150 mm, the largest deflection only increased 4 % (i.e. −106 mm to −110 mm) during the heating phase; however, the residual deflection increased 12 % (i.e. −77 mm to −86 mm) during the cooling phase. This is due to, with the increasing slab thicknesses, the self-weight of concrete slabs increased; however, the sectional stiffness also increased, which enhanced the resistance of concrete slabs under bending. According to the results, during the heating phase, the "advantages" (i.e. enhancing section stiffness) may outweigh the "disadvantages" (i.e. increasing self-weight) of the increasing slab thicknesses.

Fig. 29 presents deflections of the Slab5 which is 140 mm thickness with different steel reinforcement mesh fabrics, i.e. A193, A252, B385 (baseline), B503 and B785. As shown in Fig. 29, the maximum deflection of Slab 5 decreased "linearly" with the increasing reinforcement ratios. For example, with the increasing reinforcement ratios, 0.35 % (A193), 0.46 % (A252), 0.7 % (B385), 0.91 % (B503) and 1.43 % (B785), the largest deflection of Slab5 at mid-span was decreased linearly, as −127 mm, −123 mm, −117 mm, −107 mm and −92 mm, respectively. This is due to the increase in reinforcement ratio causing an increase in load-carrying capacity of the concrete slabs, especially for the crack control of the composite floor [69]. When the concrete slabs are under fire exposures with thermal gradients, the larger reinforcement ratio is able to provide higher yield and ultimate strengths of the slabs. Decreasing the spacing of rebars is found to be more effective to decrease the deflection of the concrete slabs under travelling fire. For example, in the

Table 3
Summary of the case studies, considering the role of slab under the baseline travelling fire scenario for the thermal and structural response and corresponding failure criteria (values in bold for highlighting failure, or very close to failure).

Case No.	FE model	Slab thickness Cofraplus 60 (mm)	Steel reinforcement (BS 4483 Fabric Reference)	Critical temperature (°C)		Critical deflection L/20 (mm)		Stress utilisation $\sigma_0/f_{y,20}$ °C	
				Beam (550)	Slab unexposed (140+20)	Beam (−300)	Slab (−300)	Beam yield stress (355MPa)	
								Tension	Compression
1	2D	–	–	***548***	–	−152	–	0.55	−0.60
2*	3D	140	B503	***549***	133	−95	−107	0.63	−0.53
3	3D	120	B503	***548***	***166***	−91	−106	0.52	−0.50
4	3D	130	B503	***549***	148	−94	−107	0.59	−0.52
5	3D	150	B503	***549***	122	−97	−110	0.68	−0.57
6	3D	140	A193	***549***	133	−114	−127	0.60	−0.46
7	3D	140	A252	***549***	133	−104	−123	0.68	−0.50
8	3D	140	B385	***549***	133	−100	−117	0.61	−0.49
9	3D	140	B785	***549***	133	−84	−92	0.64	−0.57

* Case 2 is the baseline scenario.

comparison between A252 and B503, the reinforcement ratio was doubled by adopting B503 (i.e. 0.46 % to 0.91 %), correspondingly, the largest deflection decreased 13 % (i.e. −123 mm to −107 mm).

6.3. Analysis of parametric studies

The role of slabs for predicting the structural responses and corresponding failure under travelling fire scenarios was investigated. The summary of the results is presented in Table 3. It was found that: 1) the 2D model predicted larger deflection than the 3D model (i.e. approx. 60 % larger), however, the 2D model underestimated the potentially high internal forces compared with the 3D model. This indicates that the simplification for modelling the structure as a 2D frame is not always the most conservative under travelling fires; 2) for the fire design of the composite floor, the results indicate that the increased steel reinforcement ratio results in higher influence on structural responses than the effect of increasing slab thickness.

7. Conclusions

This work first validated a 3D LS-DYNA finite element structural model against the Veselí Travelling Fire Test. Then a model for a one-story prototype steel-framed building with composite floors was adapted based on the structural layout of the BST/FRS 1993 travelling fire test. The established model investigated the thermal and structural responses as a "slice" of the large open-plan office compartment. The analysis includes a range of travelling fire scenarios with different fire spread rates, fuel load densities, and inverse opening factors (IOF) using the ETFM framework. Different fire protection schemes (i.e. with/without fire protection of the secondary beams), the combined effect of design fire resistance rating (FRR) and travelling fire spread rates were also investigated. The effect of slabs on the prediction of structural responses under travelling fires was studied, via investigating the difference between a 3D FEM model with a 2D model. In addition, two key slab design parameters (i.e. thickness and steel reinforcement) were also investigated.

The following conclusions can be drawn:

(1) Based upon the 3D finite element study in this work, full heating and cooling cycles induced by the travelling fires on the structure, are suggested to be considered in the performance-based structural fire design, similarly as the experimental findings from the Veselí Travelling Fire Test [26].
(2) Based upon the baseline travelling fire scenario studied with the 3D model of the prototype structure, a single criterion is difficult to ensure a sufficient structural fire design under travelling fires. Failure criteria are suggested to cover: critical temperature, mid-span deflection as well as deflection rate, stress conditions or utilisation of the structural member capacity.
(3) To properly apply the travelling fire method for performance-based structural fire design, parameters should be carefully set up with appropriate bounds under a physically meaningful range. This is especially important under parameters such as travelling fire spread rate, due to its high influence on the thermal and the structural response. For instance, the tension stress utilisation, 0.93 at 0.5 mm/s could be decreased to 0.46 at 12.5 mm/s, whereas fuel load densities and IOF have less impact. In general, travelling fire spread mechanism is a critical research direction in the future for defining the proper travelling fire scenarios.
(4) Global structural behaviour could be fundamentally changed due to the selection of different fire spread rates in combination with the design fire resistance rating (FRR). This change is associated with the heat transfer delay caused by fire protection, especially under the travelling fires. For instance, our prototype structure under a "slow" travelling fire (e.g. 0.5 mm/s) with an increasing FRR, its failure during the cooling phase was prevented effectively due to the decrease of the tension stress utilisation of beams (i.e. 0.98 with R30 could be decreased to 0.63 with R180). However, under a relatively "fast" travelling fire (e.g. 2.5 mm/s and 12.5 mm/s), increasing FRR may not always improve the fire performance of the structure. Although the deflections of beams and slabs are decreased, once the FRR reaches a certain level (e.g. R120 and R90), the beams with increased FRR may even show slightly higher maximum stress utilisation during the heating phase. It is suggested that severe travelling fire scenarios, a "fast" travelling fire 12.5 mm/s with a very high resultant HRR 38 MW, and a "slow" travelling fire 0.5 mm/s with a modest total HRR 1.5 MW, should both be considered in the performance-based design.
(5) Maximum stress utilisation occurs in the cooling phase for most cases due to the large tensile forces, although this might be also associated with the simplification for modelling the connections as "pinned".
(6) The global structural response, or the potential structural failure mechanism, might be also affected by the layout of the structure, in combination with the FRR and the fire spread rate simultaneously.
(7) The 3D FEM model is crucial for the structural analysis under travelling fires via considering the importance of the concrete slab, since the simplification for modelling the structure as a 2D frame cannot always provide the most conservative solution. Specifically, although the 2D model usually predicts larger deflection than the 3D model (i.e. approx. 60 % larger in our case), the 2D model could significantly underestimate the large internal force (i.e. reduced by over 80 % in our case). The more conservative and realistic internal force captured by the 3D model, would suggest the connection is likely to be at a more unfavourable situation which might induce structural collapse under travelling fires.
(8) Furthermore, the structural response of the 3D model under the travelling fires is more sensitive to the 2D model. In our case, as the fire travels the largest deflection is normally at the same bay as the travelling fire near-field bay location. However, the maximum deflection of the 2D model is more likely to be at the second span, due to its structural simplification. In addition, the "internal force reversal" caused by the heating-cooling cycles of travelling fire is also more evident in the 3D model, especially for the axial force and stress utilisation.
(9) Under the same baseline travelling fire scenario, the increased steel reinforcement ratio of the slab results in apparent lower deflection, whereas the slab thicknesses has limited impact.

Credit authorship contribution statement

Zhuojun Nan: Formal analysis, Methodology, Software, Validation, Investigation, Data curation, Writing – original draft, Visualization. **Xu Dai:** Conceptualization, Methodology, Software, Validation, Investigation, Resources, Writing – original draft, Supervision, Project administration. **Haimin Chen:** Validation, Investigation, Writing – review & editing. **Stephen Welch:** Resources, Writing – review & editing, Project administration. **Asif Usmani:** Resources, Writing – review & editing, Project administration, Funding acquisition.

Declaration of Competing Interest

The authors declare that they have no known competing financial interests or personal relationships that could have appeared to influence the work reported in this paper.

Acknowledgement

This work is funded by the Hong Kong Research Grants Council

Theme-based Research Scheme (T22-505/19-N). The authors would like to express their sincere thanks to Kamila Cábová and František Wald from Czech Technical University, for providing access to the experimental data of the Veselí Travelling Fire Test. The authors also appreciate the valuable suggestions by Egle Rackauskaite from Arup, UK, during the development of the FEM model in this work. For the purpose of open access, the author has applied a Creative Commons Attribution (CC BY) licence to any Author Accepted Manuscript version arising from this submission. The authors highly appreciate for the funding from the University of Edinburgh to have this paper in gold open access.

Appendix A. Combined effect of fire resistance rating (FRR) and travelling fire spread rates

Fig. A1.

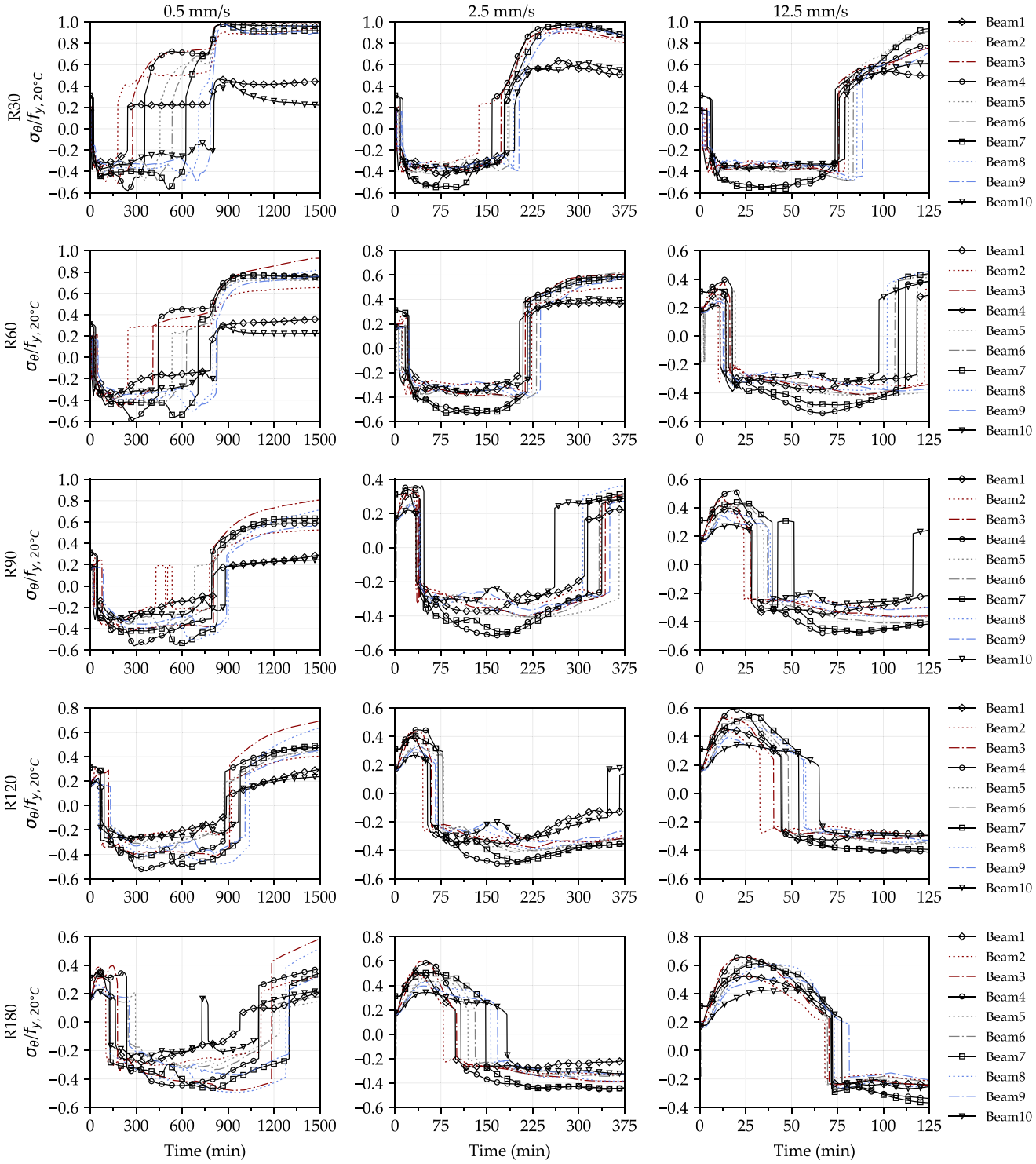

Fig. A1. Maximum beam stress utilisation at mid-span, with different combinations between FRR (R30, R60, R90, R120 and R180) and travelling fire spread rates (0.5 mm/s, 2.5 mm/s, and 12.5 mm/s).

References

[1] Franssen JM, Kodue VKR, Zaharia R. Designing steel structures for fire safety. Boca Raton, FL, USA: CRC Press; 2009.
[2] SFPE, SFPE Engineering Guide to Performance-Based Fire Protection. Quincy Mass.: National Fire Protection Association, 2007.
[3] ANSI/AISC 360-16, Specification for Structural Steel Buildings. Chicago, Illinois: American Institute of Steel Construction, 2016.
[4] ASCE/SEI 7-10, Minimum Design Loads for Buildings and Other Structures. Reston, Virginia: American Society of Civil Engineers, 2016. https://doi.org/10.1061/9780784412916.
[5] Stern-Gottfried J, Rein G. Travelling fires for structural design-part I: Literature review. Fire Saf J 2012;54:74–85. https://doi.org/10.1016/j.fire- saf.2012.06.003.
[6] Dai X, Welch S, Usmani AS. A critical review of 'travelling fire' scenarios for performance-based structural engineering. Fire Saf J 2017;91:568–78. https://doi.org/10.1016/j.firesaf.2017.04.001.
[7] Gann RG, Hamins A, McGrattan K, Nelson HE, Ohlemiller TJ, Prasad KR, et al. Reconstruction of the fires and thermal environment in World Trade Center buildings 1, 2, and 7. Fire Technol 2013;49:679–707. https://doi.org/10.1007/s10694-012-0288-3.
[8] Fletcher I, Borg A, Hitchen N, Welch S. Performance of concrete in fire: A review of the state of the art, with a case study of the Windsor Tower fire. Proc 4th Int WKSH Struct Fire, Portugal 2006:779–90.
[9] Meacham B, Park H, Engelhardt M, Kirk A, Kodur V, Straalen I, Maljaars J, Weeren KV, Feijter RD, Both K. Fire and collapse, faculty of architecture building, delft university of technology: data col- lection and preliminary analyses. Proc. 8th Int. conf. performance-based codes fire saf. des. methods, Lund, Sweden; 2010.
[10] Yarlagadda T, Hajiloo H, Jiang LM, Green M, Usmani AS. Preliminary modelling of Plasco Tower collapse. Int J High-Rise Build 2018;7(4):397–408. https://doi.org/10.21022/IJHRB.2018.7.4.397.
[11] Khan MA, Khan AA, Usmani AS, Huang X. Can fire cause the collapse of Plasco Building: A numerical investigation. Fire Mater 2022;46(3):560–75.
[12] Kirby BR, Wainman DE, Tomlinson LN, Kay TR, Peacock BN. Natural fires in large scale compartments. International Journal on Engineering Performance-Based Fire Codes 1999;1(2):43–58.
[13] Hidalgo JP, Goode T, Gupta V, Cowlard A, Abecassis-Empis C, Maclean J, et al. The Malveira fire test: Full-scale demonstration of fire modes in open-plan compartments. Fire Saf J 2019;108:102827. https://doi.org/10.1016/j.firesaf.2019.102827.
[14] Alam N, Nadjai A, Charlier M, Vassart O, Welch S, Sjöström J, et al. Large scale travelling fire tests with open ventilation conditions and their effect on the surrounding steel structure-The second fire test. J Constr Steel Res 2022;188:107032. https://doi.org/10.1016/j.jcsr.2021.107032.
[15] Charlier M, Vassart O, Dai X, Welch S, Sjöström J, Anderson J, et al. A simplified representation of travelling fire development in large compartment using CFD analyses. Proc 11th Int Conf Struct Fire, Australia 2020:526–36. https://doi.org/10.14264/5af38e2.
[16] Rackauskaite E, Bonner M, Restuccia F, Fernandez Anez N, Christensen EG, Roenner N, et al. Fire experiment inside a very large and open-plan compartment: x-ONE. Fire Technol 2022;58(2):905–39.
[17] Clifton CG. Fire models for large firecells. HERA Report 1996:4–83.
[18] Stern-Gottfried J, Rein G. Travelling fires for structural design-Part II: design methodology. Fire Saf J 2012;54:96–112. https://doi.org/10.1016/j.firesaf.2012.06.011.
[19] Rackauskaite E, Hamel C, Law A, Rein G. Improved formulation of travelling fires and application to concrete and steel structures. Structures 2015;3:250–60. https://doi.org/10.1016/j.istruc.2015.06.001.
[20] Heidari M, Kotsovinos P, Rein G. Flame extension and the near field under the ceiling for travelling fires inside large compartments. Fire Mater 2020;44(3):423–36.
[21] Dai X. An extended travelling fire method framework with an OpenSees-based integrated tool SIFBuilder. The University of Edinburgh; 2018. PhD Thesis.
[22] Dai X, Welch S, Vassart O, Cábová K, Jiang LM, Maclean J, et al. An extended travelling fire method framework for performance-based structural design. Fire Mater 2020;24:437–57. https://doi.org/10.1002/fam.2810.
[23] Rackauskaite E, Kotsovinos P, Jeffers A, Rein G. Structural analysis of multi-storey steel frames exposed to travelling fires and traditional design fires. Eng Struct 2017;150:271–87. https://doi.org/10.1016/j.engstruct.2017.06.055.
[24] Hasemi Y, Yokobayashi Y, Wakamatsu T, Ptchelintsev AV. Modelling of heating mechanism and thermal response of structural components exposed to localised fires. Thirteenth Meeting of the UJNR Planel on Fire Research and Safety 1996:237–47.
[25] Janssens ML. An introduction to mathematical fire modeling. 2nd ed. Lancaster, PA, USA: CRC Press; 2000.
[26] Horová K, Jána T, Wald F. Temperature heterogeneity during travelling fire on experimental building. Adv Eng Softw 2013;62–63:119–30. https://doi.org/10.1016/j.advengsoft.2013.05.001.
[27] Cheng X, Zhou Y, Yang H, Li K. Numerical study on temperature distribution of structural components exposed to travelling fire. Procedia Eng 2014;71:166–72. https://doi.org/10.1016/j.proeng.2014.04.024.
[28] Kallada Janardhan R, Hostikka S. Predictive computational fluid dynamics simulation of fire spread on wood cribs. Fire Technol 2019;55:2245–68. https://doi.org/10.1007/s10694-019-00855-3.
[29] Bailey CG, Burgess IW, Plank RJ. Analyses of the effects of cooling and fire spread on steel-framed buildings. Fire Saf J 1996;26:273–93. https://doi.org/10.1016/S0379-7112(96)00027-6.
[30] Moss PJ, Clifton GC. Modelling of the Cardington LBTF steel frame building fire tests. Fire Mater 2004;28(2–4):177–98. https://doi.org/10.1002/fam.868.
[31] Liew JYR, Tang LK, Holmaas T, Choo YS. Advanced analysis for the assessment of steel frames in fire. J Constr Steel Res 1998;47:19–45. http://dx.doi.org/ 10.1016/S0143-974X(98)80004-7.
[32] Röben C. The effect of cooling and non-uniform fires on structural behaviour. The University of Edinburgh; 2009. PhD Thesis.
[33] Law A. The assessment and response of concrete structures subject to fire. The University of Edinburgh; 2010. PhD Thesis.
[34] Law A, Stern-Gottfried J, Gillie M, Rein G. The influence of travelling fires on a concrete frame. Eng Struct 2011;33:1635–42. https://doi.org/10.1016/j.%20engstruct.2011.01.034.
[35] Kotsovinos P. Analysis of the structural response of tall buildings under multifloor and travelling fires. The University of Edinburgh; 2013. PhD Thesis.
[36] McKenna FT. Object-oriented finite element programming: frameworks for analysis, algorithms and parallel computing. The University of California; 1997. PhD Thesis.
[37] Jiang YQ, Kotsovinos P, Usmani A, Rein G, Stern-Gottfried J. Numerical Investigation of Thermal Responses of a Composite Structure in Horizontally Travelling fires Using OpenSees. Procedia Eng 2013;62:736–44.
[38] Rezvani FH, Ronagh HR. Structural response of a MRF exposed to travelling fire. Proceedings of the Institution of Civil Engineers-Structures and Buildings 2015;168(9):619–35.
[39] Rackauskaite E, Kotsovinos P, Rein G. Structural response of a steel-frame building to horizontal and vertical travelling fires in multiple floors. Fire Saf J 2017;91:542–52. https://doi.org/10.1016/j.firesaf.2017.04.018.
[40] Rackauskaite E, Kotsovinos P, Jeffers A, Rein G. Computational analysis of thermal and structural failure criteria of a multi-storey steel frame exposed to fire. Eng Struct 2019;180:524–43. https://doi.org/10.1016/j.engstruct.2018.11.026.
[41] Gillie M, Usmani AS, Rotter JM. A structural analysis of the Cardington British steel corner test. J Constr Steel Res 2002;4:427–44. https://doi.org/10.1016/S0143-974X(01)00066-9.
[42] Junior VS, Creus GJ, Franssen JM. Numerical modelling of a single storey industrial building at elevated temperature-comparison between 2D and 3D analysis. Mecánica Computacional 2002:1986–97.
[43] Quiel SE, Garlock MEM. Parameters for modeling a high-rise steel building frame subject to fire. J Struct Fire Eng 2010;1(2):115–34. https://doi.org/10.1260/2040-2317.1.2.115.
[44] Jiang J, Li G-Q. Disproportionate collapse of 3D steel-framed structures exposed to various compartment fires. J Constr Steel Res 2017;138:594–607. https://doi.org/10.1016/j.jcsr.2017.08.007.
[45] Jiang J, Li G-Q. Progressive collapse analysis of 3D steel frames with concrete slabs exposed to localized fire. Eng Struct 2017;149:21–34. https://doi.org/10.1016/j.engstruct.2016.07.041.
[46] Martinez J, Jeffers AE. Global structural behaviour of steel-concrete composite floor systems under travelling fires. In: Garlok M, Kodur VKR, editors. Proc. 9th Int. Conf. Struct. Fire, USA: 2016, p. 967-74.
[47] Rezvani FH, Behnam B, Ronagh HR, Jeffers AE. Robustness assessment of a generic steel fire-protected moment-resisting frame under travelling fire. Eur J Environ Civil Eng 2018;22:64–81. https://doi.org/10.1080/19648189.2016.1179679.
[48] Gernay T, Khorasani NE. Recommendations for performance-based fire design of composite steel buildings. J Constr Steel Res 2020;166:150906. https://doi.org/10.1016/j.jcsr.2019.105906.
[49] Jiang J, Lu YL, Dai X, Li G-Q, Chen W, Ye JH. Disproportionate collapse of steel-framed gravity buildings under travelling fires. Eng Struct 2021;245:112799. https://doi.org/10.1016/j.engstruct.2021.112799.
[50] Jána T, Heistermann T, Lopes F, Davison B, Simões da Silva L, Skorepa M, et al. Design of composite joints for improved fire robustness. RFCS Compfire project-final report (RFSR-CT-2009-00021), Luxembourg: European Commission, 2014. doi: 10.2777/76889.
[51] Gernay T, Franssen JM. The introduction and the influence of semi-rigid connections in framed structures subjected to fire. Fire Saf J 2020;114:103007. https://doi.org/10.1016/j.firesaf.2020.103007.
[52] LSTC, LS-DYNA. Keyword user's manual. Livermore: Livermore Software Technology Corporation (LSTC), 2007.
[53] CEN, EN 1993-1-2:2005 - Eurocode 3. Design of steel structures. General rules. Structural fire design; 2005. doi: ISBN 978 0 580 66390 1.
[54] Horová K, Wald F. Temperature heterogeneity of travelling fire and its influence on composite steel concrete floor. Civ Eng J 2015;24(1):1–10. https://doi.org/10.14311/CEJ.2015.01.0006.
[55] CEN, EN 1992-1-2:2004 - Eurocode 2. Design of concrete structures. General rules. Structural fire design. Brussels: European Committee for Standardization (CEN); 2004.
[56] Huang S, Burgess I, Davison B. A structural fire engineering prediction for the Veselí fire tests. J Struct Fire Eng 2013;4(1):1–8. https://doi.org/10.1260/2040-2317.4.1.1.
[57] CEN, EN 1991-1-1:2002 - Eurocode 1. Actions on structures. General actions. Densities, self-weight, imposed loads for buildings. Brussels: European Committee for Standardization (CEN); 2002.
[58] ArcelorMittal. Composite floor decking - Cofradal. Floors guide; 2019.
[59] CEN, EN 1991-1-2:2002 - Eurocode 1. Actions on structures. General actions. Actions on structures exposed to fire. Brussels: European Committee for Standardization (CEN); 2002.
[60] Rush D, Dai Xu, Lange D. Tisova Fire Test - fire behaviours and lessons learnt. Fire Saf J 2021;121:103261.

[61] Thomas PH, Heselden AJ. Fully developed fires in single compartments. CIB Report No 20, Fire Research Note 923. Borehamwood, UK: Fire Research Station; 1972.
[62] Dai X, Welch S, Usmani AS. Structural implications due to an extended travelling fire methodology (ETFM) framework using SIFBuilder. 10th Int Conf Struct Fire UK:2018,:455–62.
[63] Garlock ME, Quiel SE. Plastic axial load and moment interaction curves for fire-exposed steel sections with thermal gradients. J Struct Eng 2008;134:874–80. https://doi.org/10.1061/(ASCE)0733-9445(2008) 134:6(874).
[64] Yu HX, Wang HL. An assessment of the fire resistance performance of steel structures under localised fire in large open spaces. China Eng Fire Prot Tech and Fire Fighting RSQ Con 2016.
[65] IBC, International Building Code. IL, USA: International Code Council, 2018.
[66] Barrett BA. Steel Construction: Fire Protection. British Constructional Steelwork Association (BCSA): TATA Steel; 2013.
[67] Bailey CG. Membrane action of unrestrained lightly reinforced concrete slabs at large displacements. Eng Struct 2001;23:470–83. https://doi.org/10.1016/S0141-0296(00)000.
[68] Usmani AS, Cameron NJK. Limit capacity of laterally restrained reinforced concrete floor slabs in fire. Cem Concr Compos 2004;26:127–40. https://doi.org/10.1016/S0958-9465(03)00090-8.
[69] Burgess I, Chan B. An integrated yield-line approach to tensile and compressive membrane actions in thin lightly-reinforced concrete slabs. Eng Struct 2020;208:110321.
[70] Nan ZJ, Dai X, Chen HM, Welch S, Usmani AS. A numerical investigation of 3D structural behavior for steel-composite structures under various travelling fire scenarios. Proc 11th Int Conf Struct Fire, Australia 2020:599–610. https://doi.org/10.14264/a1068ab.
[71] Thomas I, Bennetts I. Fires in enclosures with single ventilation openings - Comparison of long and wide enclosures. Fire Safety Science: Proc 6th Int Symp 2000;6:941–52.
[72] Rein G, Abecassis Empis C, Carvel R. The Dalmarnock Fire Tests: Experiments and Modelling. The School of Engineering and Electronics: University of Edinburgh, Edinburgh, UK; 2007.
[73] Torero J, Majdalani A, Abecassis-Empis C, Cowlard A. Revisiting the Compartment Fire. Fire Saf Sci 2014;11:28–45.
[74] OPS2DYNA. https://github.com/Nanzhuojun/OPS2LSDYNA/releases/tag/OPS2DYNA_ThermalLoad. 2022.
[75] CEN, EN 1994-1-2:2008 - Eurocode 4. Design of composite steel and concrete structures. General rules. Structural fire design. Brussels: European Committee for Standardization (CEN); 2008.
[76] Wald F, Burgess I, Kwasniewski L, Horová K, Caldová E. Benchmark Studies, Verification of numerical models in fire engineering. CTU Publishing House 2014.
[77] Fire protection for structural steel in buildings (The Yellow Book). 5th Edition,. Association for Specialist Fire Protection; 2014.
[78] ASTM, Standard Specification for Carbon Structural Steel. ASTM A36/A36M - 19, ASTM International, West Conshohocken, PA., 2019.